Top Organomet Chem (2020) 66: 77–130
DOI: 10.1007/3418_2020_36

Published online: 26 April 2020

Earth-Abundant and Precious Metal Nanoparticle Catalysis

Margery Cortes-Clerget, Nnamdi Akporji, Balaram S. Takale, Alex Wood, Evan Landstrom, and Bruce H. Lipshutz

Contents

Abstract This chapter is an overview focusing on the preparation and use of transition metal-containing nanoparticles (NPs) described in the literature over the past decade or so. It is organized according to the metal, including NPs that feature catalysis based on Pd, Ni, Pt, Cu, Au, Rh, Ru, Co, and Fe. Nanoparticles that involve metals on various supports are discussed, as are those derived solely from precursor metals salts. Experimental procedures from these reports detailing both the preparation and use of several of these NPs are also contained herein.

M. Cortes-Clerget
Department of Chemistry and Biochemistry, University of California, Santa Barbara, CA, USA

Chemical and Analytical Development, Novartis Pharma AG, Basel, Switzerland
e-mail: margery.cortes@novartis.com

N. Akporji, B. S. Takale, A. Wood, E. Landstrom, and B. H. Lipshutz (✉)
Department of Chemistry and Biochemistry, University of California, Santa Barbara, CA, USA
e-mail: nnamdi@ucsb.edu; balaram_takale@ucsb.edu; abwood@ucsb.edu; evanlandstrom@ucsb.edu; lipshutz@chem.ucsb.edu

Exciting developments associated with mixed metal NPs and their applications that highlight synergistic effects of synthetic value offer a glimpse of what is likely to be an increasingly important direction for catalysis in the near future.

Keywords Catalysis · Nanoparticles · Synergistic effects between metals · Transition metals

1 Introduction

Metal nanoparticle technology applied to organic synthesis continues to blossom. New materials for catalysis are being introduced on a regular basis, while methods for their analyses have become increasingly sophisticated, offering insights that have led to many of these advances. Technically, even in cases where these materials are quite small, including metal clusters, metal nanoparticles (NPs), and even species containing single atoms, they are all categorized within the area of heterogeneous catalysis. A timely and extensive review by Liu and Corma in 2018 highlighted the important factors that can influence metal catalysts of these types, drawing attention to parameters such as size and shape, among several others (e.g., metal support, their chemical make-up, the influence of additives such as other metals, etc.) [1]. At stake, of course, are the resulting key issues of reactivity and selectivity and, ultimately, synthetic utility. Hence, this review focuses on not only the development of new NPs but also the synthetic applications that have appeared over the past decade, discussed according to metal.

2 Palladium

Palladium occupies a unique position among transition metals in the field of catalysis. Although a costly precious metal, it remains world-renowned for its ability to catalyze formation of new C-C bonds, such as Heck cross-coupling reactions to form new substituted olefins; the Suzuki-Miyaura, Kumada, and Stille couplings, which can afford, e.g., new biaryls; Negishi couplings that facilitate introduction of alkyl groups onto carbon sp^2 centers; and Sonogashira reactions which can afford substituted alkynes [2–8]. Moreover, gases such as CO and CO_2 can also be used in tandem with palladium catalysts to generate carbonyl-containing products [9, 10]. Palladium is also the "go-to" metal in many hydrogenation reactions [11]. The products of these numerous types of reactions oftentimes contain structural motifs present in natural products, polymers, and a wide array of pharmaceuticals and other targets within the fine chemical industry [12].

The high surface area to volume ratio of Pd NPs makes them especially reactive [13]. Heterogeneous Pd NPs as catalysts are finding increased use due to their overall stability, as avoidance of phosphine ligands on Pd in solution is readily appreciated given their potential instability, toxicity, and susceptibility to oxidation. Thus, there has been increased interest in ligand-free palladium nanoparticles. On the other hand, many examples exist where phosphines have been incorporated into palladium complexes and their derived NPs, since the presence of a ligand can significantly affect both reactivity and selectivity associated with the reaction of interest. Preparations of palladium NPs can oftentimes be straightforward and, in most cases of interest, are well documented. The flexibility in their preparation leading to NPs of different sizes and their demonstrated recyclability and catalytic efficiency make them attractive alternatives to traditional methods involving homogeneous catalysis. A general mechanistic understanding as to the exact location of catalysis in many cases, however, remains for the future [8].

A report in 2015 in *Science* disclosed that a mixture composed of an inexpensive Fe^{III} salt doped with ppm levels of Pd and a suitable phosphine ligand could be converted upon the addition of MeMgCl in THF into highly active NPs capable of catalyzing Suzuki-Miyaura couplings in micellar media under very mild conditions [14]. Each component of the catalyst proved to be critical to its activity. Anhydrous $FeCl_3$, 320–500 ppm $Pd(OAc)_2$ (relative to 0.5 mmol of halide substrate), and MeMgCl were optimal, while alternative alkyl or aryl Grignard reagents were found to afford far less effective catalysts. The inclusion of a suitable phosphine ligand, SPhos in this case, was crucial for high catalyst activity, with other phosphine ligands leading to inferior levels of conversion. This observation is of particular note, since phosphine ligands traditionally tend to play a critical role in *homogeneous* catalysis, but less so in heterogeneous processes.

Remarkably, these NPs were found to contain ca. 40% THF by weight, which was later observed to be essential for catalytic activity. TGA analysis revealed a sharp loss of mass from ca. 60 to 145°C. While the material itself maintained thermal stability from 145 to 380°C, the catalytic activity dropped precipitously after loss of THF. Analyses of these aqueous reaction mixtures by cryo-TEM revealed the association of the NPs with nanomicelles of designer surfactant TPGS-750-M (Fig. 1), where the MPEG present stabilizes the metal NPs (rods), while the (spherical) nanomicelles present deliver the coupling partners localized within

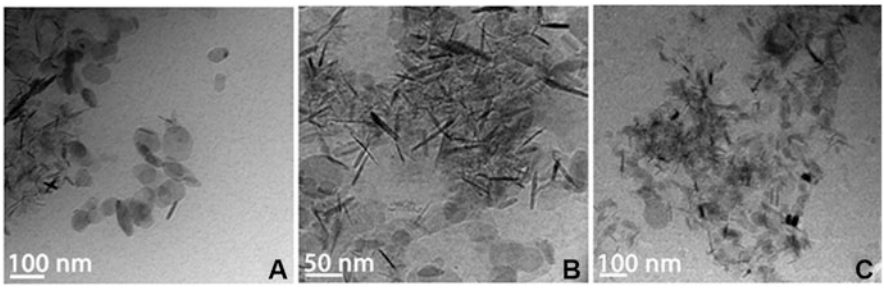

Fig. 1 Cryo-TEM images of Fe/Pd nanoparticles in the presence of aqueous TPGS-750-M

their inner cores. This so-called "nano-to-nano" effect [15] may be responsible for the observed activity, where heating is not needed notwithstanding the heterogeneous nature of the catalysis.

This NP catalyst is very effective in accommodating numerous substrate combinations. An array of functionality within either the electrophilic or boron-containing partner is tolerated, including as examples labile perfluoroarylboronic acids, complex uracil derivatives, and *O*-, *N*-, and *S*-containing heterocycles. A variety of chlorides, bromides, and iodides are amenable, while Bpin, BMIDA, BF_3K, and boronic acid reagents have all been successfully coupled using this NP catalyst under mild aqueous conditions (Fig. 2).

By replacing SPhos with XPhos and MeMgCl with MeMgBr as reductant, modified NPs are formed that can successfully catalyze Sonogashira couplings with similar efficacy on complex heterocyclic substrates [16]. This catalyst shows desirable selectivity toward oxidative addition with iodides preferentially over bromides, although in the absence of an iodide-bearing substrate, bromides can be smoothly and efficiently coupled. Notably, no copper is required in these transformations. This catalyst system was utilized in the synthesis of an intermediate en route to the antitumor agent ponatinib (Fig. 3). In all cross-coupling cases utilizing these Fe/Pd nanoparticles, residual palladium in the products is at or below the FDA threshold (10 ppm), bypassing the need for Pd scrubbing of the products.

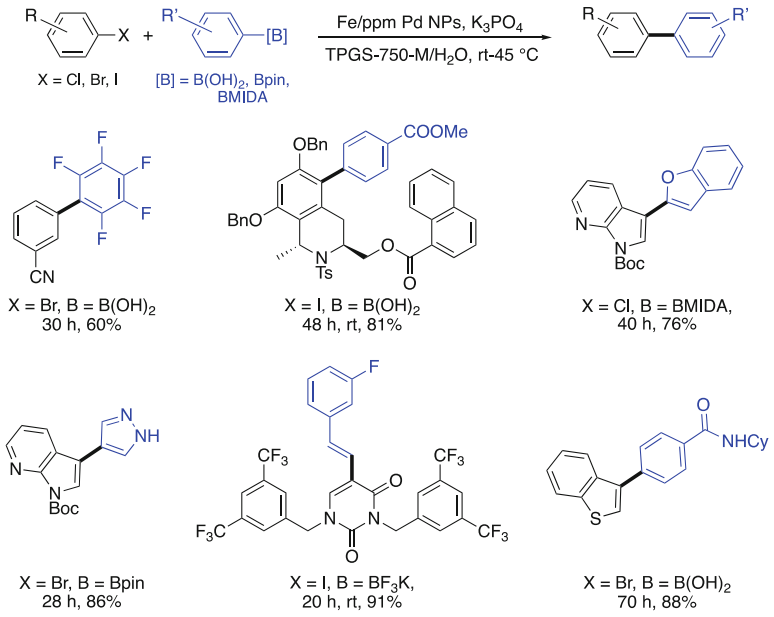

Fig. 2 Representative substrates synthesized using Fe/ppm Pd NPs

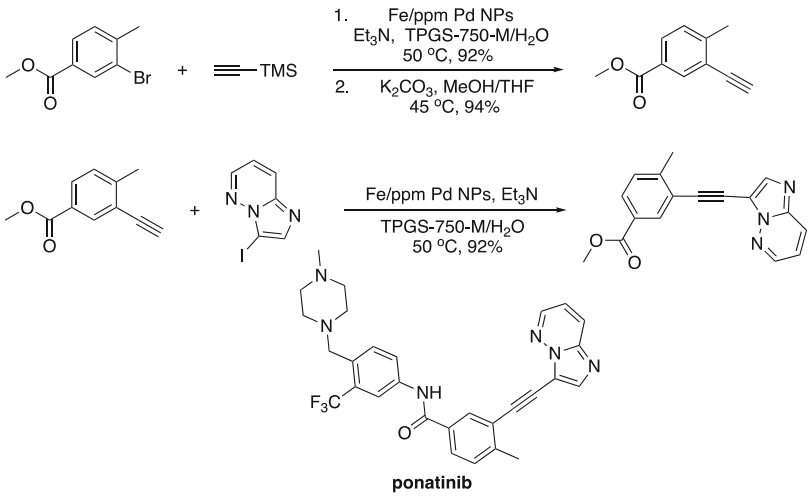

Fig. 3 Fe/ppm-Pd NPs used in the synthesis of a ponatinib intermediate

In Situ Preparation and Use of Fe/ppm Pd NPs for Sonogashira Couplings. In a flame-dried 4 mL microwave reaction vial, pure $FeCl_3$ (4.1 mg, 5 mol%) and XPhos (7.1 mg, 3 mol%) were added under anhydrous conditions. The reaction vial was sealed with a rubber septum, and the mixture was evacuated and backfilled with argon. Dry THF (1.0 mL) was added to the vial, and $Pd(OAc)_2$ (500 ppm) was then added using a 5 mM solution of $Pd(OAc)_2$ in dry THF. Then the mixture was stirred for 20 min at rt. after which dissolution and complexation of iron chloride was clearly visualized by a color change to dark brown. While maintaining an inert atmosphere, THF was evaporated under reduced pressure at rt. MeMgBr (0.25 mL, 10 mol%, 0.2 M) was added to the reaction mixture, after which it was stirred at rt. for 1 min. An aqueous solution of 2 wt% TPGS-750-M (1.0 mL) was added to the vial followed by sequential addition of an aryl halide (0.5 mmol, 1.0 equiv), alkyne (0.75 mmol, 1.5 equiv), and Et_3N (101 mg, 1.0 mmol, 2.0 equiv). The reaction vial was sealed with a rubber septum under argon and stirred at 45°C until complete consumption of starting material as monitored by TLC or GCMS. The reaction mixture was then allowed to cool to rt, and EtOAc (1.0 mL) was added and the mixture stirred gently for 1 min. The organic layer was allowed to separate from the aqueous layer with the help of a centrifuge, if needed. The organic layer was decanted using a pipette. The same extraction procedure was applied by using an additional 1.0 mL EtOAc. The combined organic extracts were dried over anhydrous Na_2SO_4. Volatiles were removed under reduced pressure to obtain crude product, which were further purified by flash chromatography over silica gel using EtOAc/hexanes as eluent.

During the screening of optimized reaction parameters for Fe/ppm Pd NP catalyzed cross-couplings, it was noted that in the absence of a phosphine ligand and with $NaBH_4$ serving as reductant, catalyst activity toward C-C bond formation was retarded in favor of reduction of nitro groups within aromatic or heteroaromatic substrates to their corresponding anilines [17]. Reductions of this functional group proceed smoothly at room temperature and pressure with only 80 ppm

Pd doped into these ligandless Fe/ppm Pd NPs. An extensive array of highly functionalized educts readily participated, leading to the corresponding amines in high yields (Fig. 4). Akin to other NPs of this type, optimal activity was realized when used in conjunction with a 2 wt% solution of aqueous TPGS-750-M. Classical methods for nitro group reductions (e.g., H_2 with Pd/C) typically require high temperatures, pressures, and catalyst loadings, necessitating specialized reaction vessels to mitigate potential safety hazards. Reductions using Fe/Pd NPs in the presence of either $NaBH_4$/KCl or KBH_4 can be accomplished without the need for any specialized equipment, allowing for ready scalability of these reactions from 0.5 mmol up to 100 mmol [18].

Nitro Group Reductions: Preparation of Fe/ppm Pd NPs In an oven-dried two-necked round-bottomed flask, anhydrous 99.99% pure $FeCl_3$ (487.5 mg, 3 mmol), $Pd(OAc)_2$ (2.2 mg, 0.01 mmol) (or other commercially available $FeCl_3$ that contains ppm levels of Pd) was added under an atmosphere of dry argon. The flask was covered with a septum, and dry THF (15 mL) was added. The reaction mixture was stirred for 20 min at rt. While maintaining a dry atmosphere at rt., 0.5 M solution of MeMgCl in THF (6 mL, 3 mmol) was very slowly (1 drop/2 s) added to the reaction mixture. After complete addition of Grignard reagent, the mixture was stirred for an additional 20 min at rt. Appearance of a yellow-brown color was indicative of generation of nanomaterial. The mixture was then quenched with pentane (containing traces of water). The THF was then evaporated under reduced pressure at rt. Removal of THF was followed by triturating the mixture with pentane to provide yellow-brown colored nanomaterial as a powder (trituration was repeated 3–4 times). The Fe nanoparticles obtained were dried under reduced pressure at rt for 10 min yielding 1.5 g Fe/ppm Pd nanoparticles. The material was used as such for subsequent reactions under micellar conditions. Note: These iron

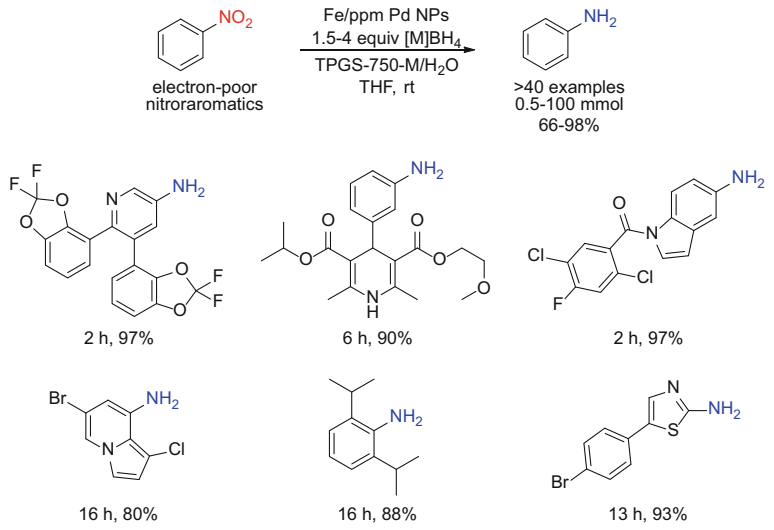

Fig. 4 First-generation Fe/ppm Pd nanoparticles for nitro group reductions

nanoparticles are best stored under argon in a refrigerator; otherwise, the color may change indicative of a drop in reactivity.

General Procedure for Reductions Iron-based nanomaterial (6 mg) was added to an oven-dried 10 mL round-bottomed flask (RBF) containing a PTFE-coated magnetic stir bar. An aqueous solution of 2 wt% TPGS-750-M (0.5 mL) was added via syringe, and $NaBH_4$ (28.5–59.0 mg, 0.75–1.50 mmol) was added to the reaction mixture. (Caution: $NaBH_4$ should be added slowly, especially for large-scale reactions, i.e., >1 mmol.) During addition of $NaBH_4$, the reaction mixture turned black with evolution of hydrogen gas. The reaction flask was covered with a rubber septum, and the mixture was stirred for 2 min at rt. The nitro group-containing substrate (0.5 mmol, pre-dissolved or dispersed in mixture of 0.5 mL aqueous TPGS-750-M and 0.1 mL THF in advance) was then added to the catalyst suspension via syringe (substrates which are not soluble in aqueous TPGS solution were first dissolved in a minimum amount of THF (160 μL for 0.5 mmol of educt)). The RBF was filled with argon and covered again with a rubber septum. Finally, the reaction mixture was vigorously stirred at rt. Progress of the reaction was monitored by TLC or GCMS. After complete consumption of starting material as monitored by TLC, the septum was removed, and argon was bubbled through the mixture. Minimal amounts of an organic solvent (EtOAc, i-PrOAc, Et_2O, MTBE, etc.) were added, and the mixture was stirred gently for 2 min. Stirring was stopped, and the organic layer was then allowed to separate, after which it was removed via pipette. The same extraction procedure was repeated, and the combined organic extracts were dried over anhydrous Na_2SO_4. Volatiles were evaporated under reduced pressure, and semi-pure product was purified by flash chromatography over silica gel. Caution: Never use acetone for TLC monitoring or column chromatography. Occasionally during the progress of the reaction, the reaction vial requires gentle shaking to avoid adherence of reaction material to the glass. Always use fresh and good quality $NaBH_4$.

Further optimization of these NPs led to an improved catalyst exhibiting synergistic effects between Pd (80 ppm) and Ni (1,600 ppm) [19]. While electron-rich nitroaromatics on occasion showed sluggish behavior toward the initially reported catalyst, the second-generation Fe/Pd/Ni NPs are, in general, far more reactive. Ether-, thioether-, and aniline-containing nitroaromatics were reduced in good-to-excellent yields with remarkable chemoselectivity (Fig. 5). For example, despite the presence of super-stoichiometric amounts of borohydride, reduction of aryl hydrazones to their corresponding hydrazines was not observed. EXAFS analysis of the first-generation NPs revealed high shell scattering indicative of tight Pd-Pd interactions. The nickel-containing particles contained no such feature. It is postulated that the presence of nickel dilutes the palladium on the surface of the NPs inhibiting clustering (i.e., Pd-Pd interactions) and therefore increasing the availability of highly reactive single atoms of Pd.

In 2018, Ming Bao and co-workers reported that allylboronates can be used as a carbon-based ligand for in situ generation of Pd NPs [20]. These have been shown to be useful in carboxylative Suzuki-Miyaura coupling reactions of benzylic chlorides with allylpinacolborate (Fig. 6). The reaction conditions were relatively

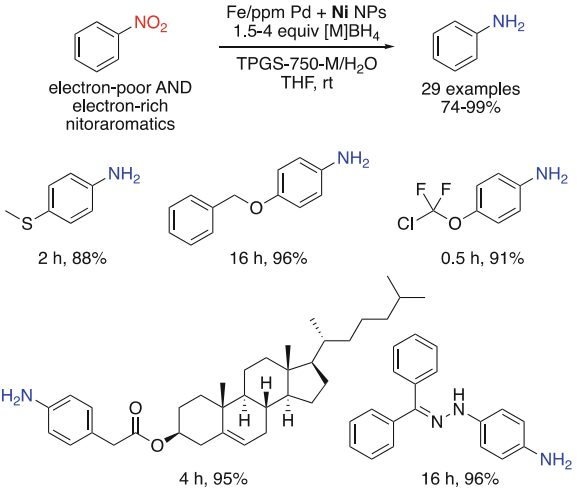

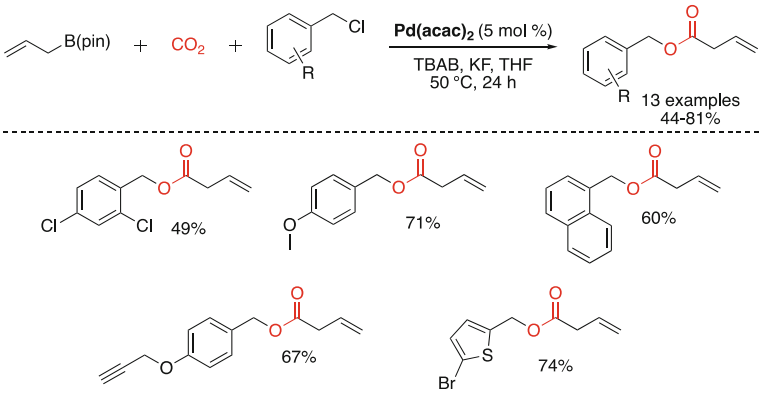

Fig. 5 Second-generation Fe/ppm-Pd + Ni nanoparticles for nitro group reductions

Fig. 6 Carboxylative Suzuki coupling reactions of benzylic chlorides with allyl borates catalyzed by palladium NPs

mild with low pressures of CO_2 compared to previous methods. Halogen atoms present on aromatic rings as part of the substrates were also unaffected, adding credence to the selectivity as well as allowing products to undergo further transformations. Electron-donating substituents on the benzene were also suitable. Thiophenes, likewise, participated in this chemistry, affording satisfactory yields.

Z-Selective semi-hydrogenations of alkynes (i.e., Lindlar reductions) have been reported using Pd NPs in water [21]. These time-honored reductions typically rely on Pd that has been "poisoned" by toxic lead and quinoline, thereby preventing over-reduction to the alkane. By contrast, this nanoparticle-nanomicelle system requires no such manipulation of the Pd catalyst. Key to the efficacy of this catalyst was the nature of both the Pd salt and the surfactant. Optimal results were achieved with 1 mol% $Pd(OAc)_2$, a 2 wt% solution of TPGS-750-M in water, and

pre-reduction of the Pd salt with 0.05 equivalents of $NaBH_4$ (followed by 0.35 equivalents for alkyne reduction). Cryo-TEM imaging of the catalyst solution revealed Pd nanoparticles (Fig. 7 – dark particles) surrounded by micellar aggregates (light gray particles). The catalyst could be generated in situ or stored for later use. Replacement of $Pd(OAc)_2$ with $PdCl_2$ and use of alternative surfactant Brij 30 with $Pd(OAc)_2$ both resulted in complete reduction to the alkane.

Of particular note is the excellent chemoselectivity associated with use of these NPs. Esters, ketones (in the presence of Pd), silyl protected alcohols, THP-protected alcohols, 1,4-unsaturated systems, Cbz-protected amines, and epoxides remained untouched during the reduction of the alkyne while proceeding in excellent isolated yields (>95%) and stereoselectivity (>95% *Z*) (Fig. 8). The catalyst and reaction medium could be effectively recycled five times without loss in efficiency. The E Factor determined for these conversions was only 3.4.

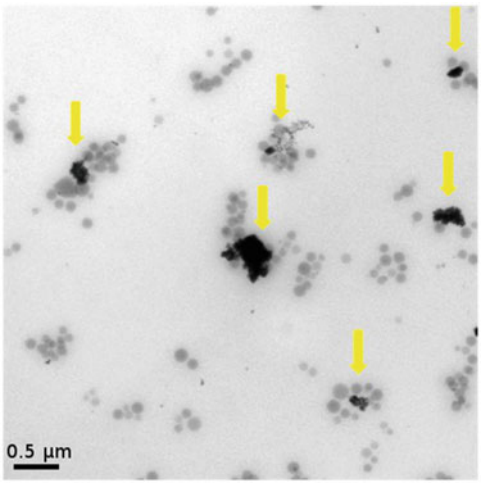

Fig. 7 Cryo-TEM image of Pd nanoparticles aggregated around nanomicelles in water

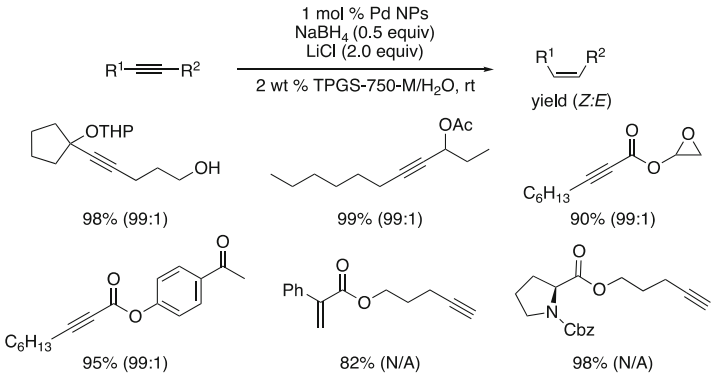

Fig. 8 Representative examples of Pd NP-catalyzed semi-hydrogenations

Roulland and coworkers [22] relied on palladium NPs for the stereo-retentive insertion of a methyl residue in their total synthesis of the aglycon of tiacumicin B. The NPs were generated in situ by mixing $Pd_2(dba)_3$ with Grignard reagent MeMgBr (Fig. 9). While stereodefined, poly-substituted alkenes are found in a wide array of drug targets and natural products [23], most routes of entry rely on nickel to catalyze couplings with alkenyl halides. In the case of a bulky leaving group like a vinyl sulfide, use of Ni-mediated substitutions has been sparse due to their sensitivity to steric hindrance around the mercaptide moiety, as well as lack of stereo-control [22]. In this case, use of NPs derived from $Pd_2(dba)_3$ in the absence of a phosphine ligand afforded the best yields. It was also noted that the vicinal unprotected hydroxyl group played an important role, potentially facilitating insertion of a Pd^0 species via chelation of magnesium between the alcoholate and the proximal sulfur atom, in turn activating the C-S bond. Transmission electron microscopy (TEM) confirmed the presence of NPs ranging from 1.5 to 2.0 nm in diameter. Reaction conditions were optimized at 1 mol% loading of palladium, since higher loadings (2.5 mol%) led to formation of undesired by-products and lower isolated yields.

Palladium nanoparticles have been used to catalyze couplings between aryllithium reagents and various aryl and heteroaryl bromides. Feringa and co-workers [24] generated these NPs in situ, and using molecular oxygen to form stable η^2-peroxo complexes, they observed rapid conversions to the coupled products on timescales of 2–5 min. Via NMR studies of intermediates and TEM analysis of the reaction medium, rapid formation of palladium NPs was observed upon addition of the organolithium. The possibility that a monoligated palladium [Pd-PR_3)] is the active catalytic species was excluded based on (a) the lack of

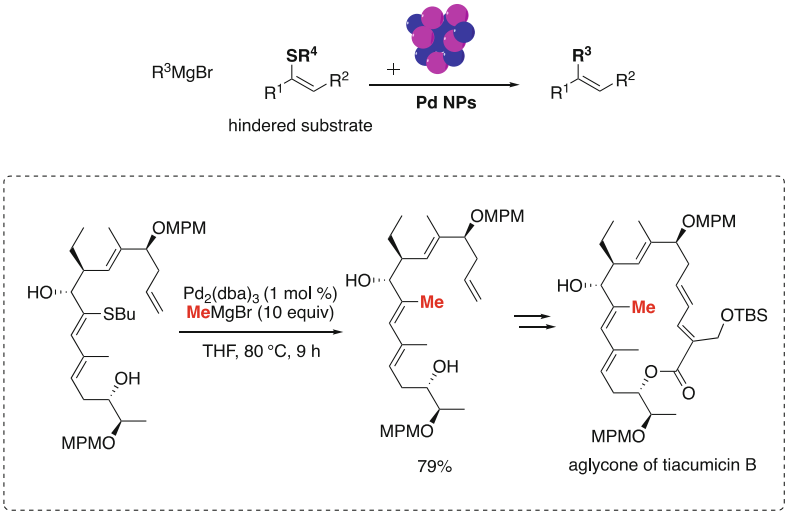

Fig. 9 Stereo-retentive cross-couplings of vinyl sulfides with Grignard reagents

reactivity with aryl chlorides, and (b) no inhibitory effect was observed from the addition of excess *t*-Bu_3P on the outcome of the cross-coupling products. Both electron-poor and electron-rich substrates gave good yields with high selectivities. The reaction proved to be selective toward aryl bromides, as aryl and benzylic chlorides present within the substrate remained untouched. Sensitive functional groups, including those bearing acidic protons, are unreactive, such as phenols, epoxides, and silyl protected pyrroles. This method was applied to time-sensitive reactions, such as synthesis of the [^{11}C]-labeled PET tracer celecoxib (Fig. 10). The expedient coupling of [^{11}C]-methyllithium to the drug precursor greatly increases the yield of the overall reaction, given the low half-life of the alkyllithium reagent ($t_{1/2}(^{11}C) = 20$ min).

Wei and co-workers showcased the ability of $Al(OH)_3$-supported palladium NPs, generated in situ, to facilitate ligand and copper-free Sonogashira and Heck cross-coupling reactions (Fig. 11, left) [25]. In their studies, they noted that nanoparticles generated in situ showed higher reactivity than catalysts prepared via co-precipitation. For Sonogashira reactions, couplings proceeded best in DMSO with the addition of TBAB (tetrabutylammonium bromide). The Pd loading was quite low at 0.2 mol% (2,000 ppm). The base also played an important role in this chemistry, as NaOAc yielded the best results over more common bases such as K_2CO_3 and K_3PO_4. The reaction ran smoothly on a range of aryl and heteroaryl bromides, including pyridines, thiophenes, and quinolines. The scope of the alkyne, however, was limited to mostly phenylacetylenes among the examples screened.

Using the same NPs, Heck reactions were also investigated, in these cases using only a 0.1 mol% loading of palladium (Fig. 11, right) [25]. A solution of TBAB in DMF was the chosen reaction medium. Both electron-rich and electron-poor aryl bromides gave the desired product using the enoate of choice, butyl acrylate. Some aryl chlorides did undergo the coupling; however, the aryl ring present contained a strongly activating nitro group. For both reaction types, high

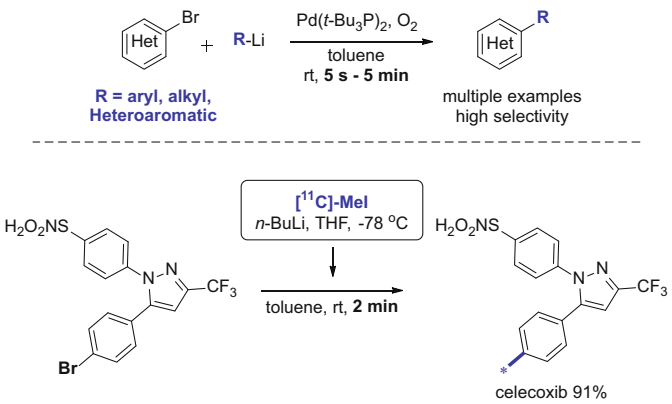

Fig. 10 Synthesis of radiolabeled celecoxib via a Pd NP-catalyzed coupling

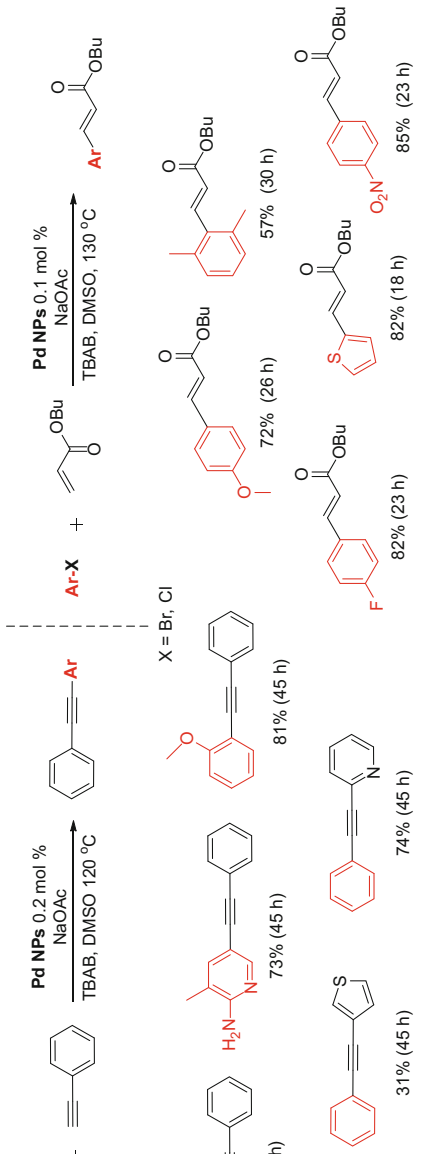

Fig. 11 Ligand and copper-free Pd NP-catalyzed Sonogashira and Heck cross-couplings

temperatures on the order of 130°C were needed. Nonetheless, the catalyst could be recovered and reused, as demonstrated for Sonogashira couplings. Membrane filtration led to catalyst recovery, which showed no apparent detriment to the yields after six consecutive cycles.

3 Nickel

There has been a significant increase in the use of nickel in synthesis over the past few decades. This can be attributed to the natural abundance of this metal which accounts for its low cost compared to that of other transition metals that are far more commonly used. Moreover, its ability to function in several oxidation states, as well as its increased nucleophilicity due to its size, has made it a desirable alternative, especially relative to palladium [26, 27]. Its place within the group 10 metals has enticed chemists to further investigate the ability of this base metal to facilitate valued organic transformations, including reductions and C-C bond formations. Substituting the more abundant nickel in reactions that mostly utilize palladium and platinum would reduce costs of various chemical processes, as well as open the door to new reactivities of the metal and its complexes.

As with palladium, use of heterogeneous nickel NPs for catalysis has gained interest for several good reasons. For example, the metal has been utilized with other metals to create bimetallic nanoparticles which appear to have a synergistic effect that can greatly contribute to the overall reactivity, as well as generality, of the reactions that it can catalyze (e.g., see Fig. 5; Fe/ppm Pd + Ni NPs).

Cai et al. introduced Ni-Co bimetallic nanoparticles (BMNPs) for chemoselective transfer hydrogenation of nitroarenes (Fig. 12) [28]. Their BMNPs were prepared in ethanol with a 1:1 mixture of nickel and cobalt salts and PVP as stabilizer. They noted that this was the ratio that afforded the best results under optimized conditions. Reduction of the metal salts to NPs with $NaBH_4$ under inert atmosphere was sufficient to form well-dispersed BMNPs with an average diameter of 2.5 nm, confirmed by TEM. The catalyst suspension was suitable for up to one week if stored

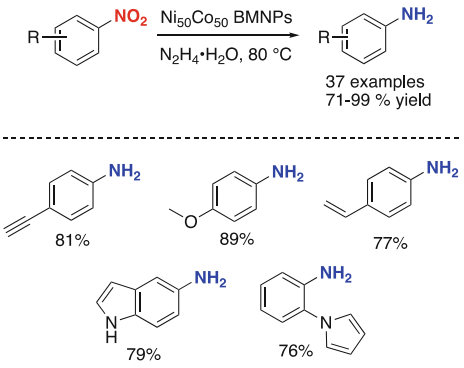

Fig. 12 Chemoselective reduction of nitroarenes by bimetallic Ni-Co NPs

under inert atmosphere. The bimetallic properties of these NPs also provided insight regarding their reactivity. They noted that the BMNPs are of a smaller particle size than the individual Ni and Co NPs, suggesting that greater surface area is available on which the reactions take place.

Hydrazine hydrate was chosen as the hydrogen donor en route to these BMNPs due to its ease of handling as well as the inert by-product formed after use. Temperature played a crucial role in this transformation; when run at 60°C, poor conversion was noted, while higher temperatures led to aggregation of the NPs resulting in reaction inhibition. A temperature of 70°C seemed to be the optimal compromise. Water or ethanol served as the reaction medium depending upon the solubility of the substrates. Electron-rich as well as electron-poor nitroarenes were smoothly converted to the corresponding amines. Halogenated anilines could also be obtained with no dehalogenation observed. Dinitro compounds were fully consumed to the desired diamine products upon addition of excess hydrazine hydrate. Most importantly, the nitro groups were reduced in the presence of olefins, alkynes, and nitrile groups indicative of the selectivity of this process. However, formyl substituents under the reaction conditions afforded the derived primary alcohol.

Preparation of $Ni_{50}Co_{50}$ BMNPs $NiCl_2{\cdot}6H_2O$ (0.5 mg), $CoCl_2$ (0.26 mg), and PVP (160 mg, average molecule weight = 40,000) were dissolved in ethanol (1.5 mL) and charged into a 10 mL reactor with a magnetic stirrer. Then, a freshly prepared ethanol solution of $NaBH_4$ (0.8 mg, in 0.5 mL in ethanol) was added into the reactor quickly under vigorous stirring (1,000 rpm) at rt. (25°C) under argon. The color of the colloidal mixture turned to black immediately which indicates that metal salts have been reduced to metal particles. The catalysts prepared were directly used for reactions, as overexposure of catalysts containing Ni to air will result in significantly decreased activity due to oxidation.

Typical Procedure Hydrazine hydrate (4 equiv) was added into the reactor which contains freshly prepared catalyst, as described above. Then, the reactor was placed into a pre-heated oil bath with a stirring speed of 500 rpm, and the substrate (1 mmol) dissolved in 1 mL ethanol was added dropwise under argon. The reactions were monitored by TLC. After the reaction, the mixture was vacuum filtered through a pad of silica on a glass-fritted funnel, and an additional 15 mL of EtOAc (5 mL portions) was used to rinse the product from the silica. The filtrate was concentrated in vacuo and analyzed by GC. Products were purified by column chromatography and identified by ^{1}H NMR and ^{13}C NMR.

Although reductive amination via metal hydrides or catalytic hydrogenation has long been reported [29], uses of hydrogen transfer to facilitate the reaction are sparse in the literature and often employ hydrazine or borohydride as the hydrogen source. However, Yus and co-workers reported that Ni NPs can catalyze reductive amination of aldehydes by hydrogen transfer using a relatively environmentally benign 2-propanol as both solvent and reductant in the absence of base (Fig. 13) [30]. Their nanoparticles were prepared by mixing anhydrous

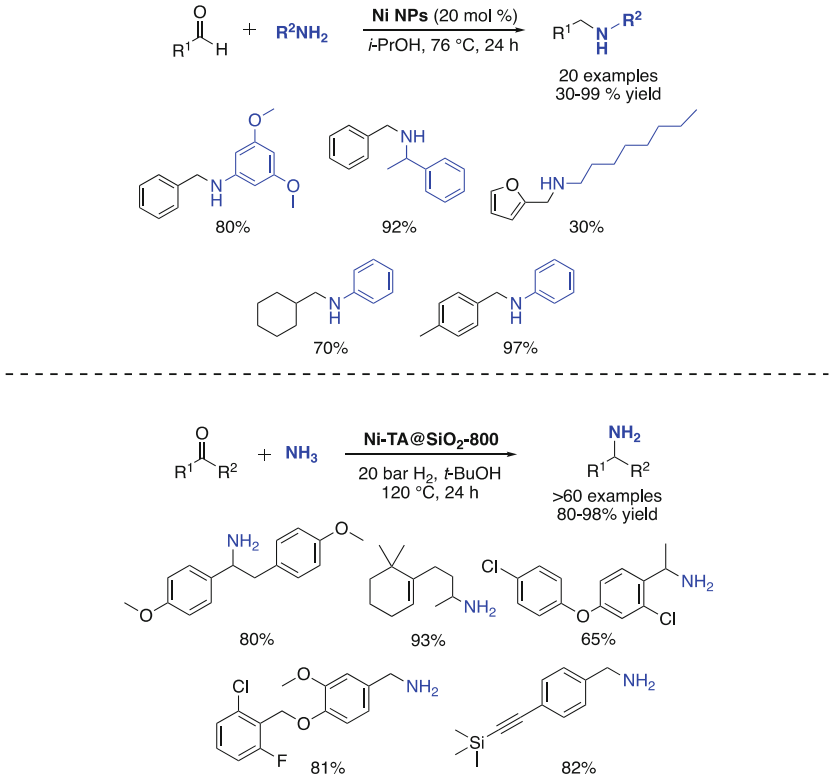

Fig. 13 Nickel NP-catalyzed reductive aminations of aldehydes

nickel(II) chloride with lithium powder and a catalytic amount of DTBB (5 mol%) in THF, which yielded NPs with an average diameter of 2.5 nm.

Reactions of benzaldehydes with primary amines and anilines smoothly afforded the desired benzylic amines under these conditions. *N*-Benzylamines, as well as *ortho*-, *meta*-, and *para*-substituted anilines, were easily obtained. Alkylamines also efficiently participated in this reaction, although phenethylamine exhibited reduced reactivity affording the corresponding product in modest yield. Substituted benzaldehydes, especially with an electron-donating component, also led to diminished yields. Advantages of this methodology include the avoidance of step-wise, preformation of the imine, as well as the source of hydrogen being both inexpensive and environmentally friendly (i.e., isopropanol). Recently, Jagadeesh and coworkers documented the scope of nickel NPs generated in situ for reductive amination [31]. Their method also allows for a range of ketones to undergo this transformation. Although their substrate scope is far more expansive in terms of complexity, the reaction requires high pressures of hydrogen as the donor and temperatures upward of 120°C.

Adholeya et al. showcased a magnetically recoverable, silica-based nickel catalyst, *Ni-TC@ASMNPs*, that could be used to catalyze Suzuki-Miyaura cross-coupling reactions [32]. The NPs were prepared via co-precipitation; iron salts were initially combined with ammonium hydroxide. Then, a coating of silica was applied in order to inhibit the aggregation of the NPs. The silica-coated NPs were then further functionalized with an NH_2 linker to provide the solid support. Finally, the material was stirred in a solution of $NiCl_2$•$6H_2O$ to form the Ni NPs which were easily separated using a magnet. Their analysis by TEM indicated an average diameter of 10–12 nm.

Upon optimization of these couplings, it was found that dioxane was the preferred solvent. K_3PO_4 was utilized as base, being far superior to other bases tested. Reaction temperatures lower than 100°C led to longer reaction times. The presence of PPh_3 was essential, as no reaction occurred in the absence of this ligand. It was postulated that the ligand may be stabilizing Ni(0) prior to oxidative addition. A range of aryl halides and pseudo-halides (Br, Cl, I, OTs) were all amenable to this transformation (Fig. 14). Aryl bromides were able to smoothly couple in good-to-excellent yields regardless of the electronic properties of the ring. Due to the magnetic properties of the NPs, the nickel catalyst could be cleanly separated from the reaction mixture using a permanent magnet. The same catalyst could be recycled for six subsequent reactions without noticeable loss of activity, as well as with negligible leaching of nickel.

Preparation of Catalyst Ni-TC@ASMNPs $Fe_2(SO_4)_3$ (6.0 g) and $FeSO_4$ (4.2 g) were dissolved in 250 mL of water and stirred at 60°C to give a yellowish orange solution. NH_4OH solution (25%, 15 mL) was added into the solution with vigorous stirring, and the color of the bulk solution turned black. Stirring was continued for another 30 min, and the precipitated MNPs were separated using an external magnet and washed several times with deionized water and ethanol.

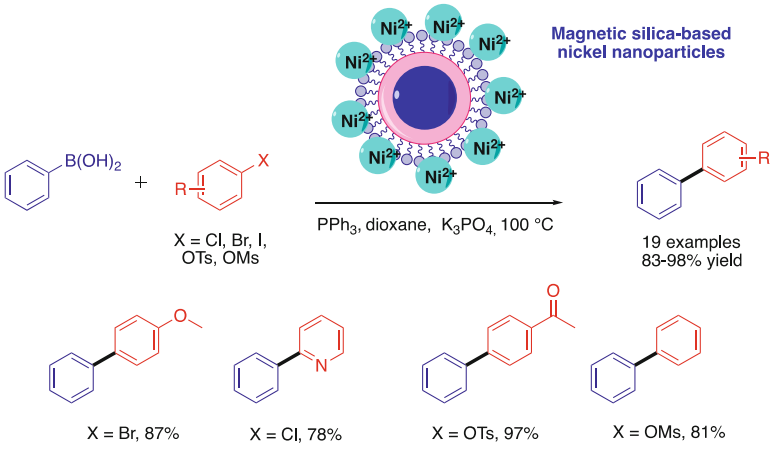

Fig. 14 Nickel-catalyzed Suzuki-Miyaura cross-couplings

Silica coating over these MNPs was achieved via a sol-gel approach. A dispersed solution of 5.0 g of activated MNPs with 0.1 M HCl (2.2 mL) in 200 mL of ethanol and 50 mL of water was obtained via sonication. Then, 5 mL of 25% NH_4OH solution was added to the suspension at rt., followed by the addition of 1 mL of TEOS, and the solution was kept under constant stirring at 60°C for 6 h. The obtained SMNPs were magnetically separated, washed with ethanol, and dried under vacuum. The obtained SMNPs were further functionalized using APTES to afford ASMNPs. This was done by adding APTES to a dispersed solution of 0.1 g of SMNP in 100 mL of ethanol under sonication, and the resulting mixture was stirred at 50°C for 6 h. For covalent grafting of the ligand on SMNPs, 1 g of ASMNP was refluxed with TC in dried methanol along with molecular sieves at 70°C for 3 h. The obtained product was washed with methanol and dried under vacuum. Finally, 1 g of grafted TC@ASMNPs was stirred with a solution of 4 mmol of $NiCl_2{\cdot}6H_2O$ in methanol for 3 h. The resulting Ni-TC@ASMNPs were separated magnetically and thoroughly washed with deionized water and dried under vacuum.

Representative Procedure for Cross-Couplings Catalyst Ni-TC@ASMNP (15 mg) was placed into an oven-dried round-bottom flask, and PPh_3 (20 mol%), aryl halide (0.5 mmol), and phenylboronic acid (0.6 mmol) were added. After this, K_3PO_4 (0.75 mmol) was added, followed by the addition of 1 mL of dioxane. The reaction mixture was kept under a N_2 atmosphere and was stirred at 100°C until completion of the reaction. The catalyst was recovered using a permanent magnet. The reaction was monitored by TLC, and the products were extracted using EtOAc, dried over sodium sulfate, concentrated under reduced pressure, and analyzed by GC-MS.

In 2015, Lipshutz et al. introduced a new nickel nanoparticle catalyst for mild and efficient Suzuki-Miyaura couplings in micellar media. This catalyst was formed by the addition of one equivalent of MeMgBr to $NiCl_2$ ligated by either dppf or dipf [33]. Cryo-TEM imaging of the NPs revealed needle-like particles situated in and around nanomicelles of TPGS-750-M (Fig. 15). It was postulated that the efficacy of these particles under the mild reaction conditions (22–45°C and 0.35 equiv. K_3PO_4) could be due to the close proximity of

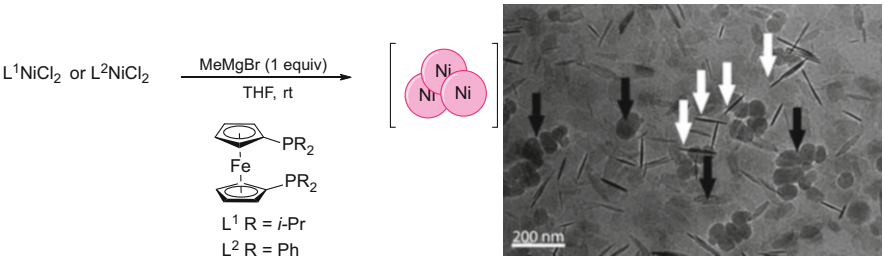

Fig. 15 Synthesis of Ni nanoparticles (left). Rod-shaped Ni nanoparticles and spherical TPGS-750-M nanomicelles (right)

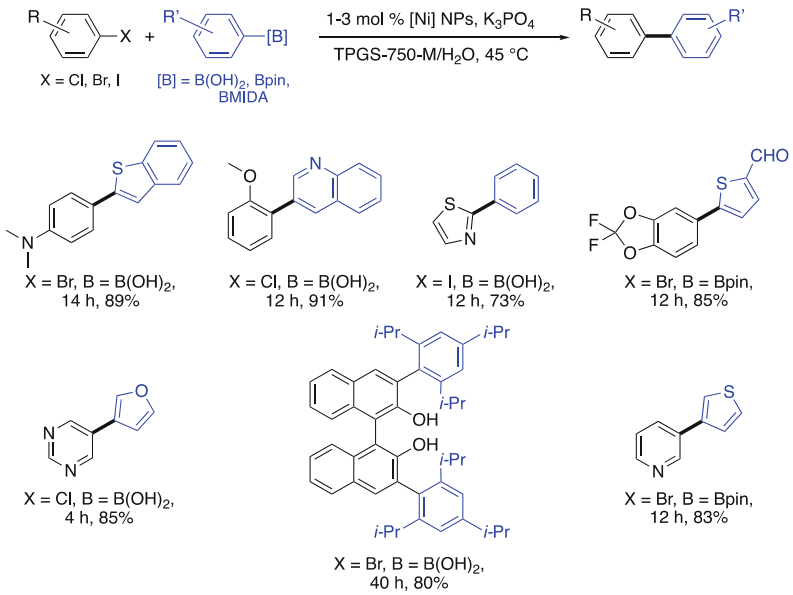

Fig. 16 Representative biaryl products prepared using Ni NPs

each type of nanoparticle, where the nanomicelles delivered relatively high local concentrations of educt to the metal NP catalyst. Counterintuitively, arylboronic esters (Bpin) were more reactive, only requiring 22°C vs 45°C for the corresponding boronic acids. The expansive substrate scope contains a wide variety of electron-rich and electron-poor aryl and heteroaryl chlorides, bromides, while the boron-containing partners included boronic acids, Bpin, and BMIDA derivatives, resulting in good-to-excellent isolated yields of products (Fig. 16). The aqueous reaction medium could be recycled six times while maintaining yields >94% (albeit with additional catalyst required) and an E Factor of only 3.8.

4 Platinum

Platinum is yet another metal that has played a crucial role in catalysis. Its use in a wide array of hydrogenation reactions as well as its applications toward various catalytic processes in the industrial setting cannot be overstated. Being the rarest of the group 10 metals, reduction in the amount of platinum utilized in chemical processes needs to be addressed. Hence, platinum nanoparticles may play a major role in addressing both the cost and endangered metal status. Bimetallic nanoparticles containing Pt have already been shown to have remarkable catalytic activity in a wide array of transformations, and further investigation into the use of Pt NPs in heterogeneous catalysis may advance their utility in organic synthesis [34].

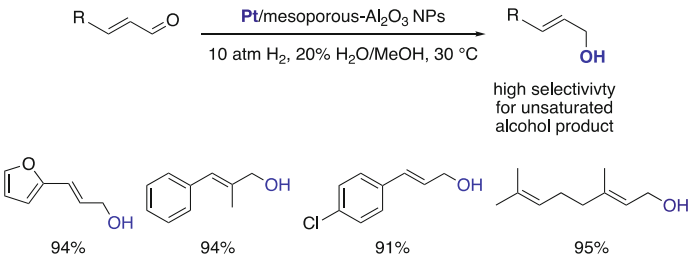

Fig. 17 Selective hydrogenation of enals

Han and co-workers utilized Pt nanoparticles immobilized on a nonporous Al_2O_3 support stabilized by aspartic acid for the selective hydrogenation of unsaturated aldehydes to allylic alcohols at room temperature (Fig. 17) [35]. Upon centrifugation of the reaction medium, the catalyst could also be recycled up to five times without noticeable decline in activity. Both the presence of aspartic acid and the nonporous properties of the support played key roles in enhancing catalyst reactivity. The aspartic acid not only inhibits formation of aggregates but also aided in the observed chemoselectivity of hydrogenation, reducing only the aldehyde over the olefin attributed to steric hindrance. The average size of the NPs according to TEM analysis was ca. 4 nm. The amount of platinum embedded in the nanoparticles, analyzed via a chemisorption method, was 0.68%.

Reaction conditions involved an atmospheric pressure of hydrogen, along with a 20% mixture of water in methanol over a ca. 3 h period. The catalyst, 30 mg, was employed for a 1 mmol scale reaction of aldehyde. Aliphatic and aromatic substrates tolerate these conditions. The reaction proceeded with selectivity of over 90% producing the unsaturated alcohol among the various substrates examined.

Like nickel, platinum, as one metal within a bimetallic NP, seems to exhibit both higher reactivity and stability as compared to the reactivity of the monometal nanoparticle counterpart. This was illustrated by work from Lee and co-workers in which they performed silylations of aryl halides catalyzed by magnetically recyclable bimetallic Pd/Pt Fe_3O_4 nanoparticles (Fig. 18) [36]. Classical introduction of the silyl moiety into organic molecules typically relies on either organolithium reagents or a Grignard reagent together with a silicon-based electrophile. This approach can be of limited scope due to base-sensitive functional groups that may be present in the molecule of interest [37, 38]. These bimetallic NPs were synthesized through a solution phase reduction process [39] that is often employed in the making of a wide array of NPs. In this case, the catalyst was composed of 4.10 wt% Pd and 9.60 wt% Pt, determined via plasma atomic emission spectroscopy.

Conditions for these silylations relied on NMP as solvent and diisopropylethylamine as base at 70°C, yielding the best results after optimization. Substrates well-suited for this method typically contained an electron-withdrawing component, as electron-rich substrates tested on both aryl iodides and bromides gave poor yields. Primarily alkylsilanes, such as triethyl- and trihexylsilane, converted smoothly to silylated aromatics in most cases, while diphenylmethylsilane led to

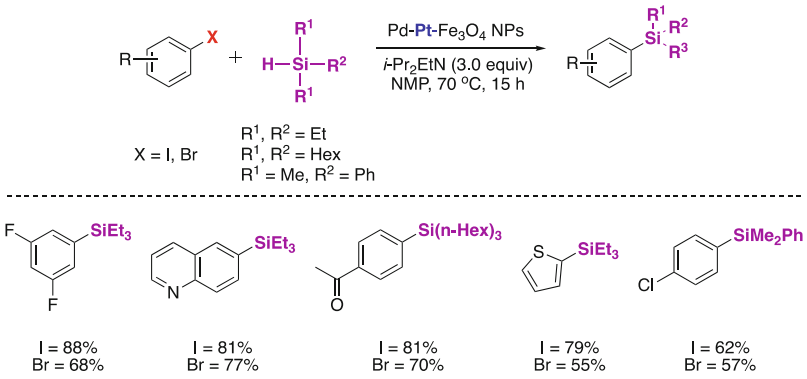

Fig. 18 Silylation of aryl halides

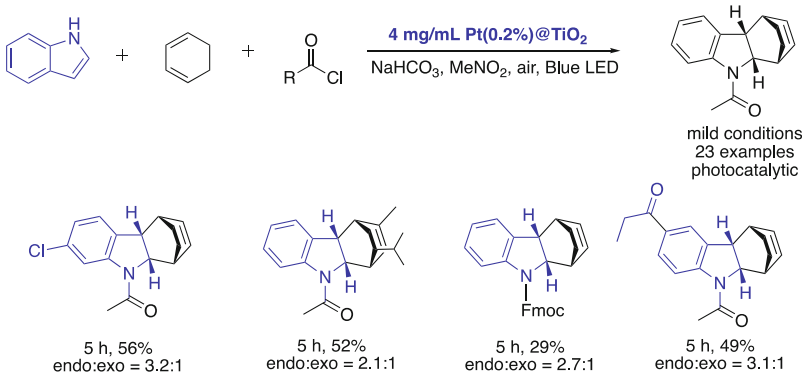

Fig. 19 Photocatalytic indole Diels-Alder cycloadditions

somewhat lower yields. With the use of a magnet, the nanoparticles could be recovered and recycled up to 20 times. It was estimated that an average of only 0.03% Pd and 0.08% Pt was lost with each recycle. Control studies with the Pd-Fe_3O_4 and Pt-Fe_3O_4 NPs showed a dramatic decrease in the rates of these reactions, as well as the amount of metal lost after each recycle (0.26% Pd and 0.55% Pt liberated), indicating the increased stability and reactivity of this bimetallic system.

Photoredox catalysis used in tandem with bimetallic NPs was studied by Tehshik et al., focused on radical cation Diels-Alder reactions of indoles [40]. Although photooxidation of indoles is well established, the common use of harsh UV irradiation can limit the reaction's scope due to functional group compatibility issues. They postulated that the use of a heterogeneous catalytic system might overcome some of these limitations, as well as introduce recyclability. Thus, the combination of a Pt(0.2%)@TiO_2 NP system together with visible light irradiation (with a 10 W blue LED) promoted generation of the desired tetrahydrocarbazoles (Fig. 19).

The presence of an acyl trapping agent was crucial, since the unprotected cycloadduct can rapidly trigger oxidative fragmentation to undesired products. Other protecting groups including Boc and Fmoc were examined, but they resulted in diminished yields. The Pt in the system was proposed to inhibit back electron transfer to the indole by acting as an electron sponge, resulting in a more efficient catalytic system. The reaction tolerates a wide range of electron-donating or electron-withdrawing functionality at the C5 and C6 positions of the indole ring. Halides, as well as a pinacolboron group, were also unreactive, opening the door to further functionalization of the cycloaddition product. It was observed that nitro- and azaindoles did not participate in this reaction. Centrifugation could be used to separate catalyst from reaction mixture, whereupon its drying under vacuum allowed for reuse in subsequent reactions. However, loss in activity was observed, most likely due to poisoning by the indole derivatives.

5 Copper

Opportunities to apply relatively inexpensive organocopper chemistry [41] in the form of nanoparticles as catalysts have also been the focus of several recent investigations. Significant efforts have been dedicated to improving the efficiency of copper located within NPs, notably toward reducing metal loading ($\leq$1,000 ppm) as well as developing an alternative to more toxic and/or precious metals. One driving force behind reducing the loading of copper can be seen in the case of biologically relevant couplings, such as the copper(I)-catalyzed alkyne-azide cycloaddition (CuAAC) or other click reactions, where excess metal may interfere with applications of the triazole products. Additionally, valuable transformations such as C-C or C-heteroatom formation as well as reduction [41] or oxidation [42] processes have been reported.

Historically, alkyne-azide cycloaddition (AAC) reactions usually lead to mixtures of 1,4- and 1,5-disubstituted triazoles. Work by Sharpless and Meldal, in 2002 [43, 44], highlighted the positive impact of adding Cu(I) to the pot, leading to regiocontrol strongly favoring the 1,4-isomer. In this regard, the emergence of CuNPs as recoverable and recyclable catalysts has begun to address the sustainability aspects of this important reaction. Radivoy et al. described both unsupported and supported CuNPs for the CuAAC reaction [45]. In the case of unsupported CuNPs, despite superior activities compared to commercial copper catalysts, the NPs had the tendency to dissolve under optimal conditions, posing a problem for recycling and residual metal to be found in the final product [46]. Later, the same group reported on supported NPs, using carbon or MagSilica. Isolation and manipulation of the organic azide needed for the Cu-catalyzed AAC could be avoided by its in situ generation via a multicomponent process from anilines, aryldiazonium salts, alkenes [47], epoxides [48], or halides [49]. Thus, both waste reduction and safer processes were achieved. Simultaneously, the CuAAC reaction could be effected in the presence of 0.5–5 mol% of CuNPs on carbon or MagSilica at 70°C in water or acetonitrile [50]. Applications of

the silica-coated maghemite (CuNPs/MagSilica) to homocoupling of terminal alkynes, as well as three-component reactions to arrive at propargylamines from aldehydes, amines, and terminal alkynes (A^3 coupling), have also been studied (Fig. 20) [49].

Astruc et al. reported PEG-2000-stabilized copper NPs [51], the formation of which required reduction of $CuSO_4 \cdot 5H_2O$ using sodium naphthalenide in acetonitrile, followed by an aqueous DCM extraction resulting in pure, stabilized copper nanoparticles (designated as Cu(0)NP-PEG). Interestingly, UV detection of the catalyst after brief exposure to air showed the formation of Cu_2O on the surface of the catalyst (designated Cu(I)NP-PEG). The activity of the three catalysts, the unpurified catalyst (Cu(0)-PEG-1), Cu(0)-PEG, and Cu(I)NP-PEG, was then used in water in a model reaction between phenylacetylene and benzyl azide at room temperature. At 50 ppm copper, a significant increase in conversion is seen using Cu(I)NP-PEG relative to that using purified Cu(0)-PEG (32%) air-free catalyst, or relative to the conversion noted using oxidized Cu(I)NP-PEG (75%). The unpurified catalyst afforded only traces of the product. Furthermore, increasing the catalyst loading of Cu(I)NP-PEG from 50 to 100 ppm resulted in 100% conversion and 97% isolated yield of the desired click product. By immobilizing the optimal oxidized catalyst onto a mesoporous type of silica (SBA-15) as solid support, syntheses of three bioactive molecules requiring only 1,000 ppm of Cu catalyst could be accomplished (Fig. 21). No leaching was detected at 50°C using a 1:1 H_2O to *t*-BuOH mixture as solvent.

In 2017, Lipshutz et al. developed a novel nanoparticle catalyst for click chemistry [52], prepared using 1,000 ppm of a Cu(I) salt in place of Pd in the Fe NPs previously described [14]. A wide variety of benzyl and alkyl azide/alkyne combinations were efficiently cyclized at room temperature. The use of 2 wt% TPGS-750-M in water facilitated the reaction of even highly water-insoluble alkynes such as those derived from α-tocopherol (84%) and solanesol (88%; Fig. 22). The active catalyst is bench-stable when stored in an aqueous medium containing ascorbic acid.

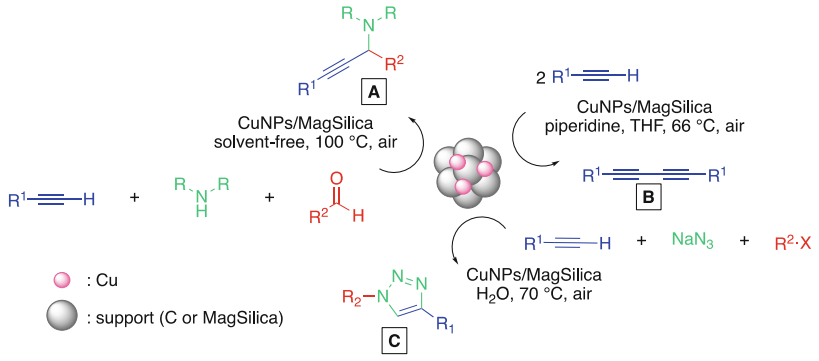

Fig. 20 CuNPs/support applied to a three-component reaction (**a**), an alkyne homocoupling (**b**), and a Cu-catalyzed AAC reaction (**c**)

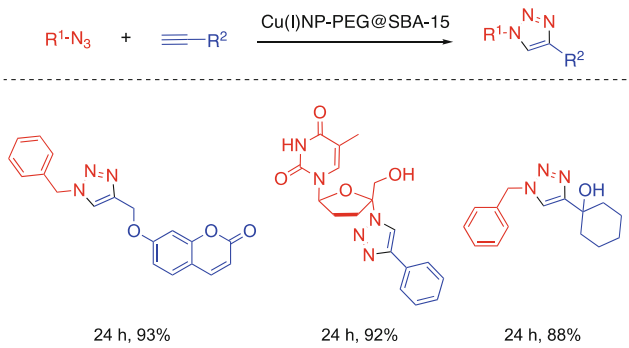

Fig. 21 ppm level of PEG-2000-stabilized CuNPs for CuAAC reactions

Fig. 22 CuAAC reactions using Fe/ppm CuNPs

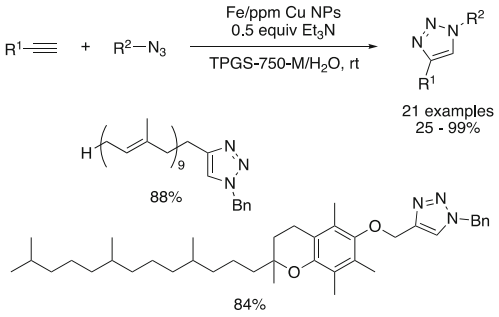

Preparation of Fe/ppm Cu Nanoparticles In a tared, flame-dried two-neck round-bottomed flask, anhydrous pure $FeCl_3$ (121.7 mg, 0.75 mmol) and CuOAc (1.839 mg, 0.015 mmol) were placed under an atmosphere of dry argon. The flask was closed with a septum, and dry THF (10 mL) was added. The reaction mixture was stirred for 10 min at rt. While maintaining a dry atmosphere at rt., MeMgCl (2.25 mL, 1.125 mmol; 0.5 M solution) in THF was very slowly (1 drop/2 s) added to the reaction mixture. After complete addition of the Grignard reagent, the reaction mixture was stirred for an additional 30 min at rt. An appearance of a dark brown coloration was indicative of generation of nanomaterial. The stir bar was removed, and THF was evaporated under reduced pressure at rt. followed by washing the mixture with dry pentane to provide a light brown-colored nanopowder. The nanomaterial was dried under reduced pressure at rt. for 10 min (603 mg) and could then be used directly for CuAAC reactions under micellar conditions. Dividing the starting mass of CuOAc by the final weight in the flask yields CuOAc concentration in the isolated catalyst: 1.839 mg CuOAc/603 mg NPs = 0.305 mg CuOAc/100 mg NPs which equates to 0.061 mg (1,000 ppm Cu for 0.5 mmol substrate)/20 mg NPs.

General Procedure for CuAAC Reactions In a flame-dried 10 mL microwave reaction vial, $FeCl_3$ (4.1 mg, 5 mol%) was added under anhydrous conditions. The reaction vial was closed with a rubber septum, and the mixture was evacuated

and backfilled with argon three times. Dry THF (0.7 mL) and CuOAc in THF (0.061 mL, 1,000 ppm; 1 g/L) were added to the vial, and the mixture was stirred for 10 min at rt., after which MeMgCl in THF (0.75 mL, 7.5 mol%; 0.5 M) was added to the reaction mixture. While maintaining an inert atmosphere, THF was evaporated under reduced pressure. An aqueous solution of 2 wt% TPGS-750-M (1.0 mL) was then added to the vial followed by sequential addition of alkyne (0.5 mmol), azide (0.6 mmol, 1.2 equiv), and triethylamine (0.0349 mL, 0.25 mmol, 0.5 equiv). The mixture was stirred vigorously at rt. After complete consumption of starting material, as monitored by TLC or GC-MS, EtOAc (1 mL) was added to the reaction mixture, which was then stirred gently for 5 min (NOTE: vigorous stirring or shaking in the reaction flask or in a separatory funnel during the extraction process resulted in the formation of an intractable emulsion with consequent reductions in isolated yields). Stirring was stopped, and the organic layer was separated with the aid of a centrifuge. The organic layer was removed, and the extraction process was repeated two additional times. The combined organic layers were dried over anhydrous magnesium or sodium sulfate or flushed through a plug of dried silica gel. The solvent was then evacuated under reduced pressure to obtain crude material which was purified by flash chromatography over silica gel using EtOAc/hexanes as eluent.

Among the virtues associated with supported NPs is their assumed re-isolation and reuse once a reaction is complete, indicative of a greener and potentially sustainable process. However, their small size may, upon filtration, block the filter pores or may not be retained at all. Magnetic separation of an active core catalyst dispersed onto a ferromagnetic surface may solve this problem. In this scenario, the nanoparticle catalyst would be simply retained on a magnet, while the bulk product mixture is separated from the system.

In that vein, Hosseini and co-workers reported the use of silica-coated Fe_3O_4 NPs applied to click chemistry [53]. The surface of the stabilized NPs was modified with a polymer [3-(trimethoxysilyl)propylmethacrylate/ILs] matrix for immobilization of copper sulfate. The cycloaddition between azides and alkynes was performed with only 0.2 mol% of catalyst, in water at room temperature affording products with yields typically surpassing 82% (Fig. 23).

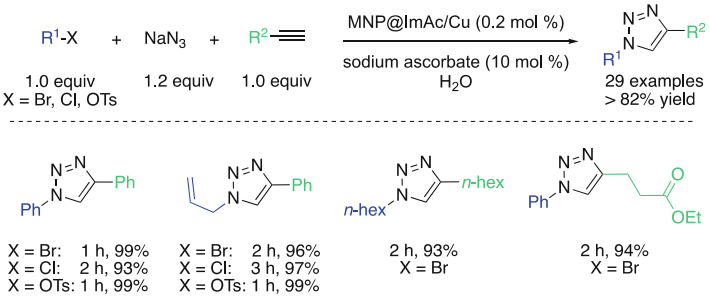

Fig. 23 Copper-loaded polymeric magnetic nanocatalysts for CuAAc reactions

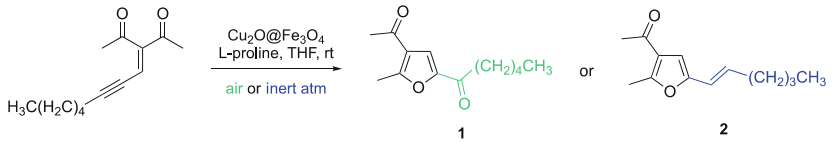

Fig. 24 Rearrangement of a diketoenyne catalyzed by magnetic CuNPs

Further advancement of related NP technology has been pursued by Liu et al. recently using magnetic, iron-supported cupric oxide nanoparticles for rearrangements of a diketoenyne to substituted furans [54]. They began by testing an array of copper (II) salts dispersed onto Fe_3O_4 as support, finding that Cu_2O led to the most active catalyst for the formation of diketofuran **1**. Further optimization using additives such as L-proline and solvent such as THF resulted in formation of the intended product **1**, along with side product **2**. Interestingly, they discovered that the atmosphere of the reaction played a crucial role: running the reaction under air resulted in the highest yield (88%) of **1**, while using an inert atmosphere afforded the highest yield of **2** (89%) (Fig. 24).

Evaluation of substrate scope for both types of optimized domino processes leading to furans indicated that high yields are formed in general, in reactions leading to *bis*-keto products **1**(78–87%), while keto-olefin products **2** formed in yields ranging from 41 to 87%. In terms of NP recovery, the catalyst was found to be deposited onto the magnetic stir bar leading to 99% recovery. Remarkably, the recovered catalyst could be reused eight more times, resulting in only a modest drop in yield of **1** under standard conditions to 72%. The results of this report, as well as those from others pursuing similar magnetic NP technology, provide industrially interesting prospects at the process level due to these facile, economical, and "green" methods that have been developed of late.

Mesoporous polymers (MP) have also attracted a lot of attention due to their large surface area and their high stability to acidic and basic conditions. Zhang et al. described a green synthesis of mesoporous polymer-supported CuNPs and their applications to a Sonogashira-like reaction between acyl chlorides and terminal alkynes [55]. These NPs were obtained via melt infiltration of copper nitrate hydrates into a phenol-formaldehyde polymer, followed by a pyrolysis-induced reduction of Cu(II) ions. Subsequent use of a capping agent or additional reduction process was not needed. This catalyst was used for the synthesis of seven alkynes under mild conditions (solvent-free, 40°C) with good-to-excellent yields (71–99%; Fig. 25). The coupling provides access to ynones, a structural array found in several natural products. The material can be recycled at least six times with no decrease of reactivity. ICP analysis revealed that only 0.17% Cu had leached from the catalyst after ten cycles, making it a good candidate for pharmaceutical applications.

CuNPs have also been utilized for reduction processes. Notably, the original work from Zamani et al. involved use of renewable and low-cost biomass containing cellulose and lignin as the support. Indeed, crushed walnut shells have been used to support and stabilize the metal (Fig. 26) [41].

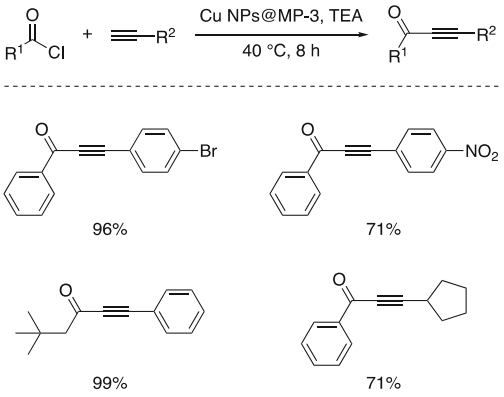

Fig. 25 Sonogashira-like reaction catalyzed by CuNPs supported on a mesoporous polymer

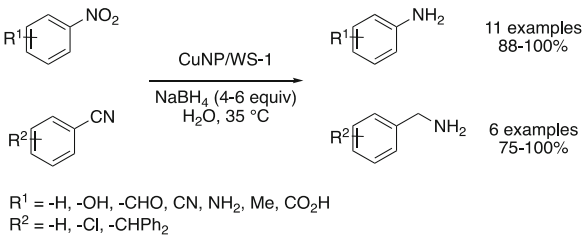

Fig. 26 Copper nanoparticles on walnut shell for reduction reactions

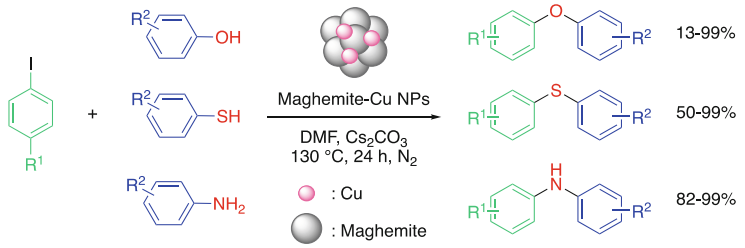

Fig. 27 C-Heteroatom bond formation with Cu-maghemite NPs

Gawande et al. reported the use of magnetic CuNPs for various C-heteroatom bond constructions [56]. Copper was uniformly dispersed on the surface of maghemite thereby gaining access to new C-O, C-S, and C-N bonds in moderate-to-excellent yields despite high temperatures and catalyst loadings (~3–6 mol%). These NPs could be recovered magnetically, washed with ethanol, dried at 60°C under vacuum, and then reused six times with unaltered efficiency (Fig. 27).

One-pot, multicomponent reactions (MCRs) are of great industrial importance, offering expeditious routes toward complicated target molecules, as illustrated by Ugi [57, 58], Passerini [59], Biginelli [60, 61], and others. The processes involved usually enjoy the benefits of environmental friendliness, as the number of downstream processing and purification steps is typically significantly reduced.

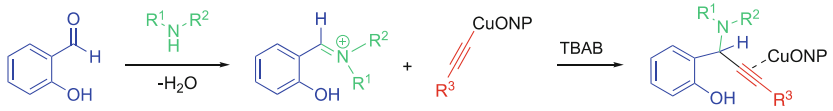

Fig. 28 Reaction between 2-hydroxybenzaldehyde, a secondary amine, and an alkyne catalyzed by Cu(I) oxide NPs

Fig. 29 Solvent-free synthesis of substituted benzofurans catalyzed by Cu(I) oxide NPs

Therefore, the combination of both MCR and non-noble nanoparticle catalysis, as well as neat reaction conditions, represents a synthetic strategy as a means to "green-up" an approach to functionalized, complex cores. A recent example of the combination of MCR and copper(I) oxide NPs was described by Sharghi et al. for construction of functionalized benzofurans [62]. This involved a three-step, one-pot process, wherein a secondary amine condenses onto a salicylaldehyde, forming an iminium intermediate in the presence of tetra-*n*-butylammonium bromide (TBAB), followed by 1,2-addition of a copper-(NP)-acetylide to form the corresponding tertiary amine (Fig. 28).

Key to this sequence is the combination of the deprotonation of the phenol along with activation of the alkyne by the copper nanoparticles. Subsequent 5-exo-dig cyclization affords the immediate precursor to the final aromatic benzofuran product (Fig. 29).

Optimization of the catalyst for this transformation led to copper(I) NPs as the best source of copper, compared to copper(II) salts. The nanoparticles were then prepared using a route developed by Tang et al. [63, 64]. Screening solvents showed that the reaction run neat at 100°C gave the best result for the cyclized product (91% yield) in less than 2 h. Recycling of these nanoparticles for the same reaction reduced efficiency in product formation by only 8% after five consecutive runs (90% yield for the first run, 82% for the fifth run). Analysis of the catalyst showed loss of copper of 7% after five runs. Ultimately, this reaction provides an example of the combination of two "green" technologies: multicomponent reactions and low-cost copper NP catalysis.

6 Gold

Heterogeneous gold catalysts as used in organic synthesis have appeared in three main forms (Fig. 30). These are not only different in appearance and reactivity but also in their preparation. The first two, metal clusters and Au NPs on a

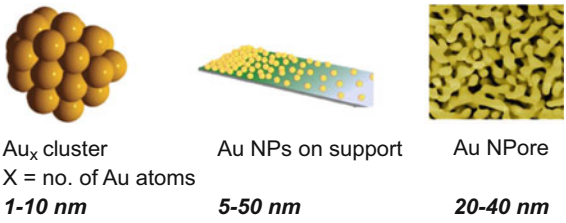

Fig. 30 Heterogeneous gold catalysts

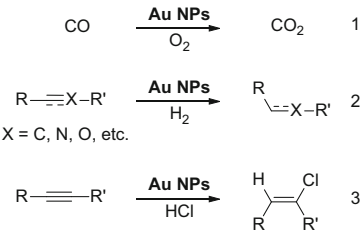

Fig. 31 Heterogeneous gold catalysis

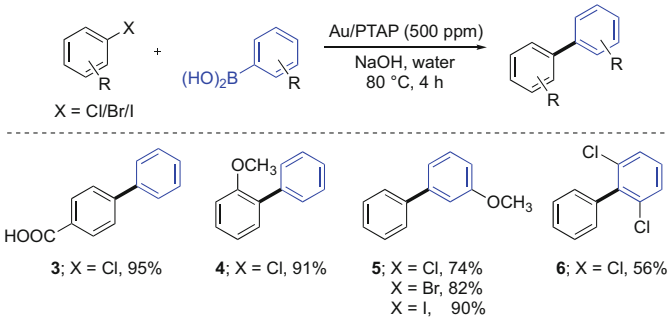

Fig. 32 Heterogeneous gold catalysis

support, are prepared from metal salts, while the third is prepared essentially from bulk gold possessing silver or other less noble metal impurities [64, 65].

The most notable applications of gold catalysis were mainly based on fundamental reactions (Fig. 31), such as CO oxidation (Eq. 1) [66, 67], hydrogenation (Eq. 2) [68–71], and hydrochlorination of alkynes (Eq. 3) [72]. These heterogeneous reactions have been widely investigated and reviewed over time. What has been most intriguing of late, however, is how gold NPs function as an alternative to copper, palladium, or other transition metals for C-C and C-N couplings, in addition to other complex catalytic reactions (vide infra).

Suzuki-Miyaura (SM) coupling reactions are highly dominated by palladium catalysts, attributed to the extensive work done on fine-tuning of ligands that allows for couplings of even especially challenging reaction partners. On the other hand, gold has only recently been introduced for this purpose by Guo et al. [73] who reported the first gold nanoparticle-mediated SM couplings of aryl halides (chlorides, bromides, and iodides) with boronic acids (Fig. 32). Nanoparticles

of ca. 1 nm in size were supported or stabilized by polyaminothiophenol (PTAP) and were easily prepared by mixing the appropriate precursors. Reactions could be performed in water using only 500 ppm of gold catalyst, albeit at 80°C. Although trace amounts of gold were leached into the solution leading to debate regarding the homo- vs. heterogeneity of the reaction, the catalyst was recycled six times without noticeable differences in chemical yield. The chemistry can be done with electron-poor (**3**) or electron-rich (**4**) chlorides. The normal reactivity trend of I > Br > Cl was also followed to arrive at product **5**. A bulky, *di-ortho*-halo-substituted boronic acid also gave product (**6**), although in this case the yield was modest. The size of gold NPs has considerable effect on the reactivity, where 5 nm gold particles led to only trace amounts (ca. 10%) of product.

Preparation of the Polymer-Supported Au Catalyst 2-Aminothiophenol (100.0 mg, 0.4 mmol) was dispersed in aqueous HCl solution (1.0 M, 20 mL) with magnetic stirring at rt. for 1 h to obtain a uniform solution. After that, the mixture was maintained at 20°C for 0.5 h before oxidative polymerization. Then, a quantitative amount of an aqueous $HAuCl_4$ solution (0.1 M) was added to the above mixture in one portion. The resulting solution was stirred for another 0.5 min to ensure complete mixing, and then the reaction was allowed to proceed with agitation for 24 h at 20°C. Finally, the product was washed with deionized water until the filtrate became colorless and then dried under vacuum at 60°C for 24 h.

General Procedure for Suzuki-Miyaura Cross-Coupling The aryl halide (225.0 mg, 2.0 mmol), phenylboronic acid (292.6 mg, 2.4 mmol), and NaOH (320.0 mg, 8.0 mmol) were added to 40 mL of deionized water. The solution was stirred at 80°C until the chemicals were completely dissolved. Then, an aqueous solution of the Au catalyst (1.0 mM, 1.0 mL, 0.05 mol%) was added to the stirred solution in one portion, and the reaction mixture was stirred for another 4 h at this temperature. After the mixture had cooled to rt., the organic product was extracted with Et_2O (3 × 20 mL). The organic layer was dried with anhydrous Na_2SO_4. After filtration, all volatiles were removed under reduced pressure to yield the final product.

Following this initial discovery, applications of Au NPs toward SM couplings have gained attention from the synthetic community (Table 1). In this context, Corma, Garcia, and co-workers [74] used Au-platelets grafted on graphene (Au/*fl*-G) for SM couplings of aryl halides with phenylboronic acid in water (entry 1). Interesting is the reactivity of aryl halides in the order of Cl > Br > I, which is contrary to expectations based on C-X bond strength. DFT calculations suggested that such reactivity could be observed due to a poisoning effect of halide on gold, with iodide having a greater effect than bromide and much higher than chloride. Thomas et al. [75] prepared a composite of gold NPs with strontium, cross-linked alginate carboxymethyl cellulose, and graphene oxide (Sr/Alg/CMC/GO/Au) and utilized 50 ppm of this catalyst for SM couplings of chlorobenzene with phenylboronic acid in water at 80°C, leading to a 76% yield of the desired product (entry 2). Nemygina et al. [76] have

Table 1 Au NPs for Suzuki-Miyaura couplings

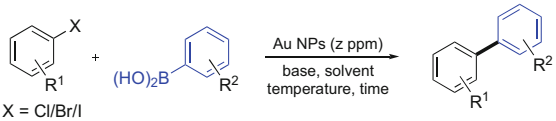

Entry	Au NPs (ppm)	X/R^1/R^2	Base	Solvent	Temperature (ºC)/ time (h)	Yield (%)
1	Au/fl-G (N/A)	CI/H/H	NaOH	H_2O	80/24	65
2	Sr/Alg/CMC/GO/Au (50)	CI/H/H	NaOH	H_2O	80/4	76
3	Au-Pd/HPS (N/A)	Br/4-Ome/H	NaOH	EtOH/ H_2O	60/3	71
4	Fe_3O_4-Au@SF-SBA-15 (6400)	CI/H/H	K_2CO_3	EtOH/ H_2O	80/1.3	95

Table 2 Au NPs used for Heck and Sonogashira couplings

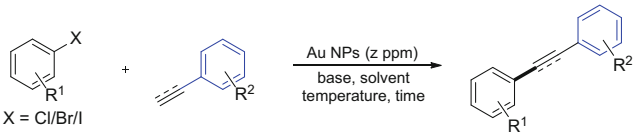

entry	Au NPs (ppm)		X/R^1/R^2	base	solvent	temperature (ºC)/time (h)	yield (%)
1	Au-Pd NPs-1 (2000)	*Heck*	I/H/H	K_2CO_3	H_2O	80/8	94
2	Au-Pd NPs-2 (2000)		Br/H/H	K_2CO_3	H_2O	80/12	85
3	Au/SiO2 (30,000)	*Sonogashira*	I/H/H	K_2CO_3	DMF	~130/4	87
4	Au/Pd_2-Sn NRs (N/A)		I/H/H	KOH	DMF	130/0.5	67

shown that bimetallic Au-Pd core-shell NPs stabilized with hyper-cross-linked polystyrene (Au-Pd/HPS) could be used for SM couplings of 4-bromoanisole with phenylboronic acid in an EtOH/water mixture at 60°C under light irradiation using a 300 W filament lamp (entry 3). Very recently, Khodaei and Dehghan [77] explored comparatively complex Fe_3O_4-Au@SF-SBA-15 NPs for couplings of chlorides, bromides, and iodides at 80°C in aqueous ethanol (entry 4). In this case, recycling this catalyst seven times showed limited reduction in yield.

Gold catalysis using NPs is also applicable to both Heck and Sonogashira reactions, which are alternative ways of preparing internal alkenes and alkynes, respectively (Table 2). Nasrollahzadeh et al. [78] used 2,000 ppm Au-Pd bimetallic nanoparticles (Au-PdNPs-1), prepared by reducing gold and palladium salts using *Euphorbia condylocarpa* plant extract, for Heck couplings between aryl iodides and styrene derivatives in water at 80°C (entry 1). The catalyst was reused over four cycles, giving essentially the same chemical yields. Moreover [79], they also prepared bimetallic Au-Pd nanoparticles (Au-PdNPs-2) by

electrochemical reduction of the corresponding salts. Interestingly, 3,000 ppm of metal within these NPs was sufficient to catalyze Heck couplings of bromides under close to the same conditions as used for Au-PdNPs-1 (entry 2). The authors did not perform control experiments with only Au NPs or Pd NPs; hence, the need for a bimetallic system is still an open question. Experiments that test the extent of leaching of metals, however, were carried out to establish the heterogeneous nature of these reactions.

De Souza et al. [80] have used 3 mol% (30,000 ppm) gold nanoparticles supported on silica (Au/SiO_2) for copper-free Sonogashira couplings of iodobenzene with phenylacetylene under microwave conditions in DMF (entry 3). This educt gave an 87% yield of the alkyne within 1 h, while bromobenzene afforded a 61% yield and required a longer reaction time (3.5 h). Recently, Nafria et al. [81] used gold nanoparticles supported on Pd_2-Sn nanorods (Au/Pd_2-Sn NRs), prepared by growing gold dots on nanorods for Sonogashira coupling between iodobenzene and phenylacetylene in hot DMF (entry 4). Apart from the desired product, both partial and complete reduction of the initially coupled product alkyne was observed, where the hydrogen for reduction was coming from DMF.

Three-component couplings that rely on gold NPs involve 1-pot, 2-bond (C-C/C-N) formations leading to highly valued propargylamines [82]. As examples, this reaction represents a key step in the synthesis of an intermediate toward the naamine family of natural products [83], as well as a lactone intermediate used to prepare other natural products (Fig. 33, left) [84]. The mechanism of this reaction is believed to be similar to that of other metal-catalyzed A^3 couplings. Aurophilic interaction of Au NPs with the alkyne leads to formation of a Au-acetylide complex, which then attacks an iminium ion formed from the amine and aldehyde to give the desired product, releasing the Au NPs. In the process, a molecule of water is lost (Fig. 33, right).

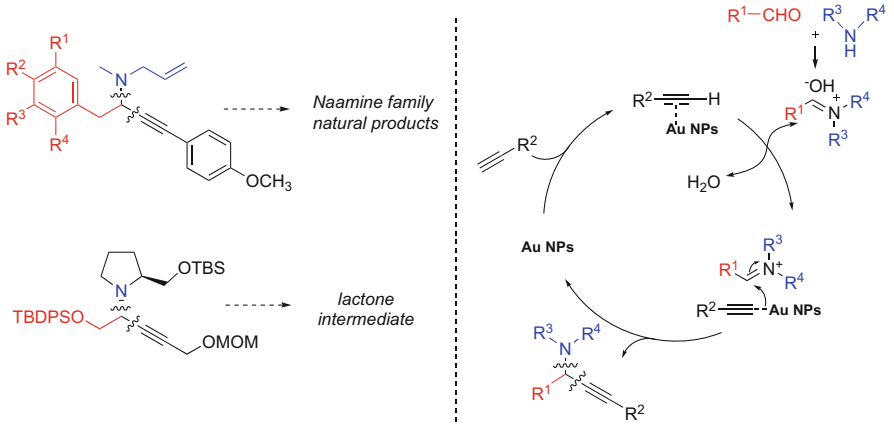

Fig. 33 Targeted products using Au NPs (left) and a proposed mechanism of A^3-couplings (right)

Although the mechanism is not fully established, considerable research has been done in this regard on heterogeneous gold catalysts following the first report by Kidwai and co-workers [85]. In this work, gold NPs of varying sizes (10–70 nm) were prepared. It was then observed that Au NPs of size 10 nm showed the best activity. The only drawback anticipated was the need for excessive amounts of these NPs (10 mol%), used in methanol at 75–80°C. Nevertheless, a wide variety of substrates was studied (Fig. 34; e.g., **7**), most affording excellent chemical yields. Following this discovery, Huang et al. [86] used robust gold NPs supported on thiol-modified cellulose nanocrystallite Au/HS-CNC (4.4 mol%) for this same reaction type but under solvent-free conditions to arrive at a wide variety of propargylamines (e.g., **8**) in good-to-moderate yields. In 2016, Haruta's [87] group prepared phosphine-/phenylacetylide-protected gold clusters on TiO_2 ($Au_{25}(PPh_3)_{10}(PA)_5X_2$)/$TiO_2$ and applied these to A^3 couplings in water at 100°C to give the desired product in 90% yield (see **9**). Yields were similar for the first (90%) and second (88%) recycles. This catalyst has been applied to several substrates leading to products in good-to-excellent yields, although in the case of aliphatic aldehydes, yields dropped significantly (~30%). Recently, Veisi and co-workers [88] described an eco-friendly method to prepare Au NPs by reducing gold salts with *Stachys lavandulifolia* (Au/*S. lavandulifolia)*. Such nanoparticles were utilized for similar A^3-couplings to give a variety of products (e.g., **10**).

Corma and Hashmi [89] reported that gold nanoparticles supported on CeO_2 (Au/CeO_2) could be utilized for alkyne activation of ω-alkynylfurans, leading to the cyclized phenols in high yields (Fig. 35). Analysis of the extent of leaching showed that 25 ppm of gold had been released into solution, questioning heterogeneity of the reaction.

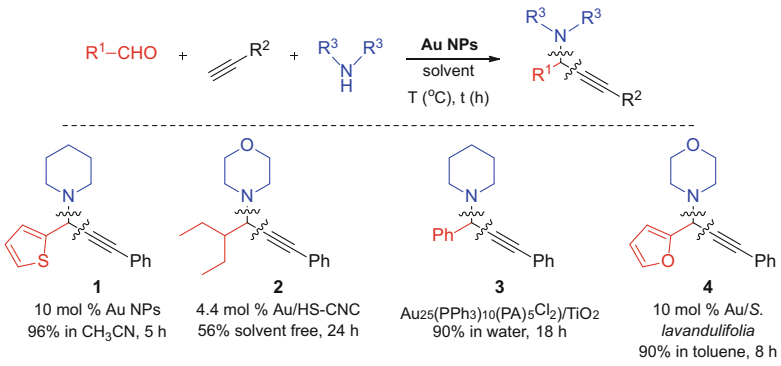

Fig. 34 Representative examples of A^3-coupling using different Au NPs

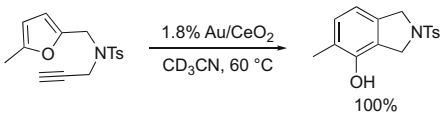

Fig. 35 Cyclization of alkynylfuran to phenol using Au NPs

Oh and Han [90] described spherical monodispersed Au(III) NPs for use in a cascade-type cyclization, leading to an interesting polycyclic ring system (Fig. 36). The mechanism proposed is akin to that characteristic of homogeneous gold catalysis. Alkyne activation with gold leads to a zwitterionic intermediate, which further undergoes [3 + 2] cyclization with the tethered allene to give the final oxabicyclic product.

Stratakis and co-workers [91] used 1.2 mol% of TiO_2-supported Au NPs (Au/TiO_2) for cyclization of enynes (Fig. 37). The desired product was obtained in 92% yield after a 4-day reaction period. The mechanism was found to involve a cyclopropyl gold carbene complex, which then undergoes ring expansion and isomerizes to the desired product by eventual loss of the Au catalyst.

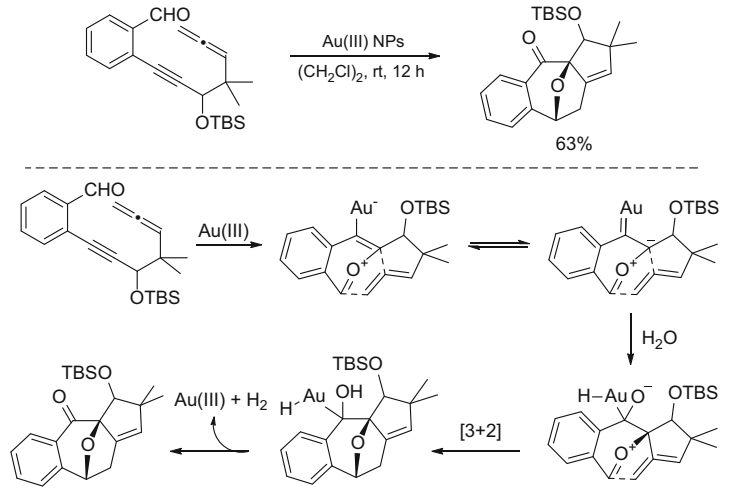

Fig. 36 Cascade intramolecular cyclization of an alkynyl benzaldehyde + allene using Au NPs

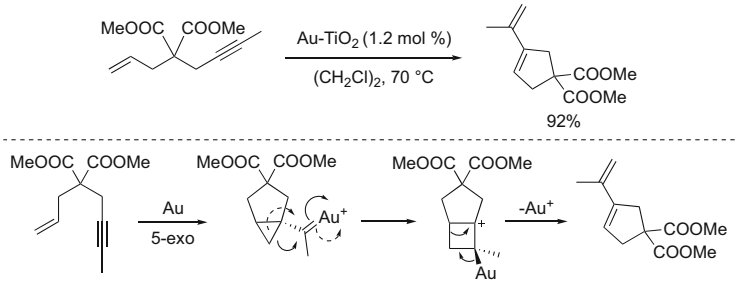

Fig. 37 Cycloaddition of enynes using Au NPs

7 Rhodium

Given that rhodium is among the rarest and most expensive precious metals, use of heterogeneous Rh NPs as highly reactive, robust, and reusable platforms can be especially attractive, perhaps most notably in the pharmaceutical industry where the residual contamination by Rh is limited to <100 μg/day (oral PDE) [92].

While Suzuki-Miyaura and Sonogashira cross-couplings are dominated by Pd-catalyzed processes, some examples mediated by Rh have been reported [93–95], illustrating the versatility of rhodium NPs. Most applications described, however, involve hydrogenation and hydroformylation reactions.

In 2016, Karakulina et al. described the cooperative effect of Rh NPs and acidic ionic liquids (ILs) for the chemoselective reduction of quinolines, as well as pyridine and benzofuran derivatives, to access the corresponding heterocycles [96]. To avoid harsh conditions (i.e., temperatures >150°C, high catalyst loadings, etc.), a chlorozincate-[bmim][BF_4] IL medium was found not only to stabilize and support the NPs but also to participate in the reaction. It is postulated that the Lewis acid IL coordinates to the heteroatom and facilitates hydrogenation of the ring under milder conditions (80°C, 30 bars of H_2). Indeed, in the absence of the chlorozincate, lower conversions were observed (Fig. 38). Both electron-donating and electron-withdrawing substituents, as well as halides, are well tolerated. The catalyst has been recycled six times without substantial loss of reactivity (90 → 84%, over 6 cycles). This method is remarkable given its chemoselectivity, as the aromatic rings remained untouched, leading to reduction of only the heteroaromatic.

The work of Kobayashi and co-workers involves Rh/Ag bimetallic NPs stabilized by nanocomposites of cross-linked polystyrene-based copolymers, and carbon black has been introduced as a new strategy for Rh immobilization [97]. This polymer-incarcerated metal platform (PI/CB Rh/Ag) shows high catalytic activity, robustness insofar as recyclability and reactivation are concerned, and no metal leaching. A first application of this system to asymmetric 1,4-additions of

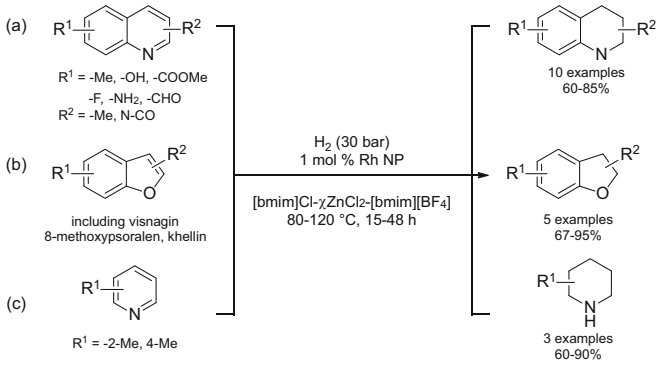

Fig. 38 Rh NP/[bmim]Cl-χ$ZnCl_2$-[bmim][BF_4] ($c = 0.67$) catalyzed hydrogenation of quinolines (**a**), pyridine derivatives (**b**), and benzofuran derivatives (**c**)

arylboronic acids to enones has been reported [98]. A bifunctional chiral diene ligand was used to simultaneously bind the metal and activate the substrate through Brønsted acid activation. While *(S)*-BINAP was initially investigated, a significant amount of Rh leaching was observed, ultimately suppressed by the use of this diene ligand (Fig. 39) [99]. The proximity of the substrate to the metal and the bulkiness of the chiral ligand allowed the reaction to proceed with high yields and stereoselectivities. Compared to homogeneous systems, the heterogeneous NPs showed superior performance, even with a lesser amount of ligand (0.05 mol % vs. 0.11 mol%). Use of a bimetallic system impacted greatly the surface distribution of Rh. Indeed, STEM analysis and EDS mapping revealed aggregation of Rh within the monometallic Rh NPs, while rhodium was more dispersed in the bimetallic Rh/Ag system.

Several examples, including three biologically important molecules, were prepared using this approach. Recycling of the NPs (up to six times) showed no significant loss of reactivity or selectivity. Comparison between heterogeneous and homogeneous catalysis showed that, despite a long induction period for the NP version, they are stable and ultimately lead to completion even at lower concentrations, while use of homogeneous catalysis plateaued, leading to lower yields. The mechanism is postulated to follow a redox process between the arylboronic acid and the surface of the NPs, as the induction period was reduced by incubation with the NPs. Coordination of the ligand to the reduced surface may then follow different pathways. In the case of hydrogenation, the reaction would happen directly at those sites, but in the case of C-C bond formation, the mechanism is more controversial. A smaller entity could detach from the NPs as a form of an active metal cluster or complex, which could reaggregate as NPs after the reaction. The second theory suggests that some degree of homogeneous metal complex leached into solution. As no leaching was detected by inductively coupled plasma (ICP) or a hot-filtration test, the latter hypothesis is unlikely [100].

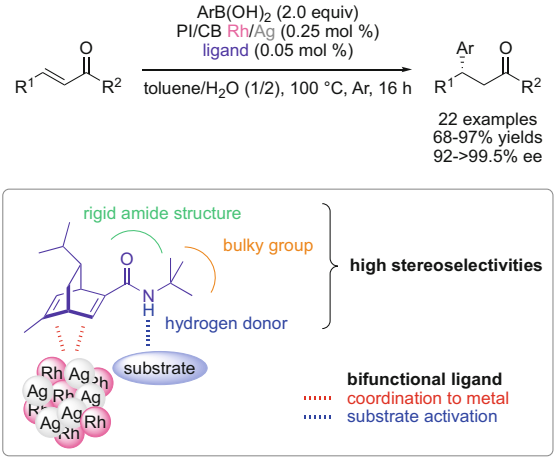

Fig. 39 Asymmetric 1,4-addition reaction with PI/CB Rh/Ag NPs and bifunctional ligand

The same system has been applied to asymmetric arylations of imines (Fig. 40) [101]. Aryl tosylimines substituted by electron-withdrawing or electron-donating groups can be arylated in high yields and stereoselectivities. In the case of aliphatic imines, being more prone to hydrolysis, an induction period to activate the catalyst at 100°C in the presence of the arylboronic acid (reductant) helped to diminish this side reaction and led to the desired products with 99% ee's despite low yields. The NPs could be recovered by simple filtration and reused, along with ligand addition and reactivation at 150°C, up to five cycles.

Use of heterobimetallic NPs is also of high interest as they usually show improved performances compared to the monometallic NPs, alone, or combined. The same group recently reported Rh/Pt NPs, supported on alumina and polysilane (DMPSi), for hydrogenation of arenes (Fig. 41) [102]. The NPs have been used both in batch and under flow conditions. Very high activity was observed in the batch system, under mild conditions (0.00625 mol%, 30–50°C, 1 atm H_2). These Rh-Pt/(DMPSi-Al_2O_3) NPs could be recycled via simple filtration and reused ten times. In the case of decreased activity, drying the NPs under argon was sufficient to reactivate them. Even greater activity was noted when applied to flow processes, especially for highly coordinating substrates.

Prof. Chung and co-workers have extensively studied the application of Co/Rh heterobimetallic nanoparticles in carbonylation-related reactions (Fig. 42) [103, 104]. These NPs were prepared by mixing $Co_2Rh_2(CO)_{12}$ and $Co_3Rh(CO)_{12}$ clusters in a solution of *o*-dichlorobenzene, oleic acid, and trioctylphosphine oxide at 180°C, over 2 h. After removal of solvent, the resulting NPs were suspended in THF and either used directly or immobilized by refluxing them in

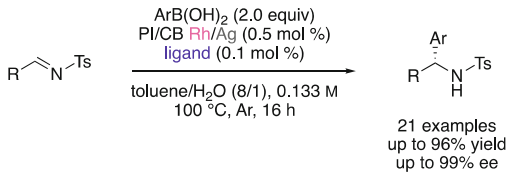

Fig. 40 Asymmetric arylations of imines catalyzed by PI/CB Rh/Ag NPs

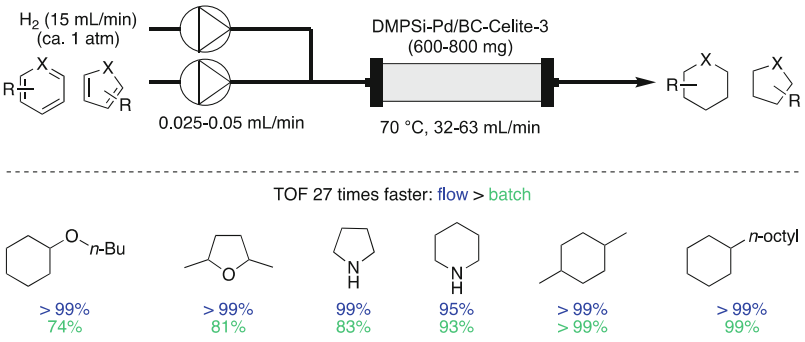

Fig. 41 Arene hydrogenation catalyzed by Rh-Pt NPs under batch and flow conditions

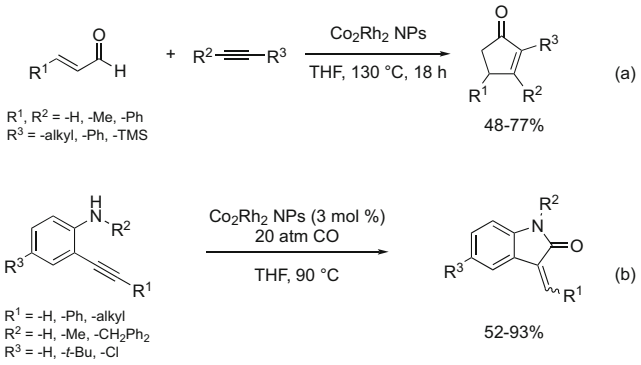

Fig. 42 Co_2Rh_2 NPs as catalysts for carbonylation-type reactions: (**a**) Pauson-Khand-type reaction using an olefinic aldehyde as CO source; (**b**) carbonylation cycloaddition of 2-alynylanilines to oxindoles

THF in the presence of flame-dried charcoal for 12 h, followed by filtration and then drying. As determined by ICP-AES, the ratios of Co:Rh were 1.09:1 and 2.93:1, respectively [105].

Application to [2 + 2 + 1] Pauson-Khand cycloaddition reactions confirmed the synergistic effect of these bimetallic structures. Indeed, the intramolecular reaction of allyl propargyl ether under one atmosphere of CO afforded 87 and 88% yields, with Co/Rh and supported CO/Rh NPs, respectively. The solid support did not affect the outcome of the reaction and allowed five recycles without significant loss of reactivity. On the other hand, no reaction was observed with supported Co/C NPs, and low-to-moderate yields were reported using (Rh_4) and Co_3Rh/C (23 and 65%, respectively). A mixture of both Co NPs and Rh NPs led to only 12% yield, confirming the synergistic effect. Perhaps more important than the recycling aspect of this technology is the residual amount of metal found in the final product. ICP-AES elemental analysis showed less than 0.1 ppm of leached metals after reaction completion. The FDA limitation for the orally permitted daily exposure for Rh and Co in drugs is 100 and 50 μg/day, respectively. These NPs have also recently been applied to reductive aminations [106, 107] and reductive cyclizations to access indoles [108].

8 Ruthenium

Ruthenium has an especially broad number of oxidation states and, thus, various coordination geometries, making it a versatile catalyst. Hara et al. reported aminations of carbonyl compounds in the presence of ammonia as nitrogen source and hydrogen gas as reductant, catalyzed by highly active and structurally controlled ruthenium NPs (Fig. 43) [109]. The morphology of the catalyst was the key to access primary amines with high reaction rates. Flat-shaped pristine

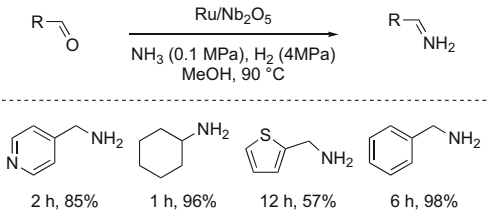

Fig. 43 Reductive amination catalyzed by Ru NPs

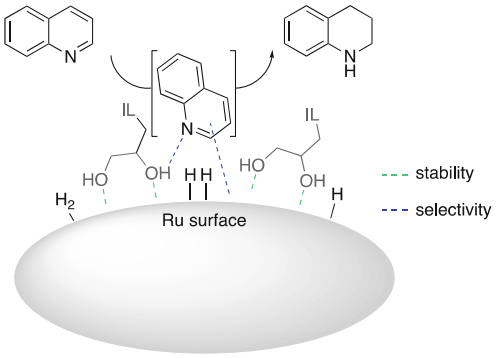

Fig. 44 Selective reduction of quinolines by Ru-diol-functionalized-ILs

fcc (face-centered cubic) ruthenium NP performance was in most cases superior to that previously described using Ru/Nb_2O_5 [110]. Indeed, reaction rates have been reported to be 5–7 times higher. While both catalysts are supported by a weakly electron-donating material, the flat Ru NPs present a larger surface of Ru(0). Functional groups such as halides, aryl, and heterocycles are well tolerated. The nanoparticles have been recycled four times without loss of reactivity.

Prechtl and co-workers have described use of ruthenium NPs in multifunctional ILs for selective hydrogenation of quinolines [111]. Here again, the nature of the IL was crucial for obtaining good selectivity. Diol-functionalized ILs have been found to play a significant role as chemoselective controllers as well as stabilizers for the hydrogenation of *N*-heterocyclic compounds. The 1–3 nm Ru NP surface is believed to be coated by the diols, which activate the heteroaromatic within the substrate (Fig. 44). In the absence of these functionalities, up to 9% of the side-product 5,6,7,8-tetrahydroquinoline was detected. Pyridines, pyrimidines, pyrroles, and pyrazoles have been successfully reduced. By contrast, indoles and carbazoles, being less basic, are less prone to be involved in hydrogen bonding with the diols and, hence, are typically fully reduced. Both methods, using Rh as reported by Dyson et al. (vide supra) [96] and Ru as catalyst for the selective hydrogenation of *N*-heterocycles, require similar conditions (pressure, temperature, reaction time), but a slightly lower loading was necessary with Rh (1 vs. 2 mol%).

Preparation of NPs for Hydrogenations A screw-capped vial with butyl/PTFE septum was loaded with [Ru(2-methylallyl)$_2$COD] (12.1 mg, 0.038 mmol) and the appropriate ionic liquid (0.3 g) under argon. The suspension was heated to 90°C and

stirred under argon for 18 h resulting in a black suspension. The NP suspension was evaporated under reduced pressure to remove volatile by-products from the decomposition of the organometallic precursor. The monometallic Ru NPs in $[C_1C_1(EG)IM]NTf_2$ were prepared adapted from a literature method using a concentration of 0.1 M precursor in the IL. The monometallic Ru NPs in $[C_2OHMIM]NTf_2$ were synthesized using 0.1 M precursor in IL suspension at 90°C for 18 h.

Representative Hydrogenation Reaction To freshly prepared Ru NPs in an IL was added 1.9 mmol of the N-heteroaromatic compound. Then, the vial was placed in a stainless-steel autoclave; the reactor was sealed, charged with hydrogen, and was then placed into a preheated aluminum heating block (600 rpm) at the appropriate temperature. For certain compounds, mesitylene was added as cosolvent for better solubility of the substrate. After the appropriate reaction time the reactor was cooled to rt. For work-up, the reaction mixture was extracted with 5 × 2 mL of n-pentane or diethyl ether, the solvent was evaporated under reduced pressure, and 20 μL (0.01 mmol) of hexamethyldisilane as internal standard was added.

9 Cobalt

Hydroquinolines are present in many pharmaceuticals and agrochemicals. While rhodium NPs can selectively hydrogenate *N*-heterocyclic compounds, an alternative approach using an earth-abundant metal under mild conditions is desirable. Beller et al. have developed cobalt oxide-derived NPs featuring nitrogen-doped (e.g., phenanthroline) graphene layers on alumina [112]. While reduction of quinoline failed using the homogeneous catalyst $Co(OAc)_2.4H_2O$/1,10-phenantroline, these NPs, obtained via pyrolysis, led to reduction of the heterocyclic ring in good-to-excellent yields (Fig. 45). The NPs have been reused six times with only a slight loss in reactivity. Hydrogenation of indoles to indolines was also reported.

Semi-hydrogenation of alkynes in the presence of hydrogen gas is an attractive route to access alkenes, for both economic and environmental reasons. Cobalt NPs have also proven to be efficient for selective semi-hydrogenation of alkynes without over-reduction to the corresponding alkanes (Fig. 46) [113]. Computational studies

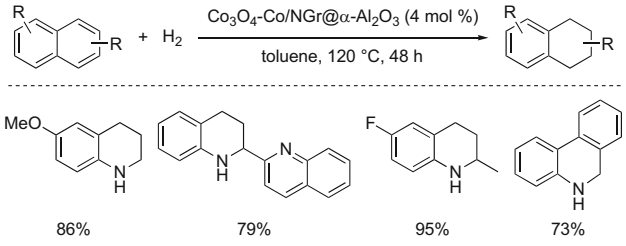

Fig. 45 Semi-hydrogenation of heteroarenes by Co NPs

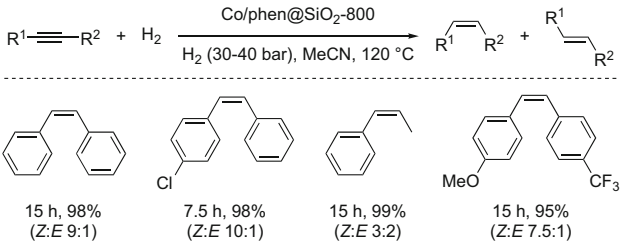

Fig. 46 Semi-hydrogenation of alkynes catalyzed by Co NPs

show that over-reduction of the alkene to the alkane is forbidden. After alkene insertion to form the alkylcobalt(I) intermediate, β-H elimination is energetically favored over protonation of the Co-C bond [114].

10 Iron

Iron, the fourth most abundant element on Earth, is attractive not only as an economical choice of metal but for its magnetic and catalytic properties. Fe(0) and iron oxides, namely, maghemite (γ-Fe_2O_3) and magnetite (Fe_3O_4), are the two dominant forms of iron NPs encountered in the literature (Fig. 47). Use of the reduced, less stable form in synthesis is still very early in its development. Indeed, Fe(0) NPs are pyrophoric upon contact with oxidizing agents; hence, working with a pre-oxidized form is far more convenient. Surprisingly, while iron is commonly used on large scale for catalytic hydrogenation (e.g., the Haber-Bosch process), its applications to pharmaceuticals and fine chemical synthesis are still minimal and should be investigated further for obvious environmental and economic reasons.

A sustainable iron-catalyzed (*Z*)-selective alkyne semi-hydrogenation in ionic liquids has been reported by Gieshoff et al. [116]. To avoid use of expensive and endangered Pd, or other platinoids or group ten metals, as well as toxic $Pb(OAc)_2$, Lindlar-type catalysts involving Fe NPs, stabilized by ionic liquids and a suitable ligand, acetonitrile, have been developed. The nanoparticles were prepared by reduction of $FeCl_3$ with EtMgCl. The presence of a nitrile function in, e.g., CH_3CN, either directly involved with the ILs or as an additive, was required to control the reactivity of the catalyst and to avoid over-reduction to the alkane. The solvent plays a crucial role here, as the ILs allow not only for catalyst recycling but also stabilization of the NPs. Indeed, the catalyst lost activity after 48 h in the absence of ILs (Fig. 48). Transmission electron microscopy (TEM) of the Fe NPs in ILs showed that their initial diameter of 4–5 nm enlarged to 8–20 nm under hydrogenation conditions. Optimized conditions were applied to numerous alkynes and are well tolerated by numerous functional groups, including free

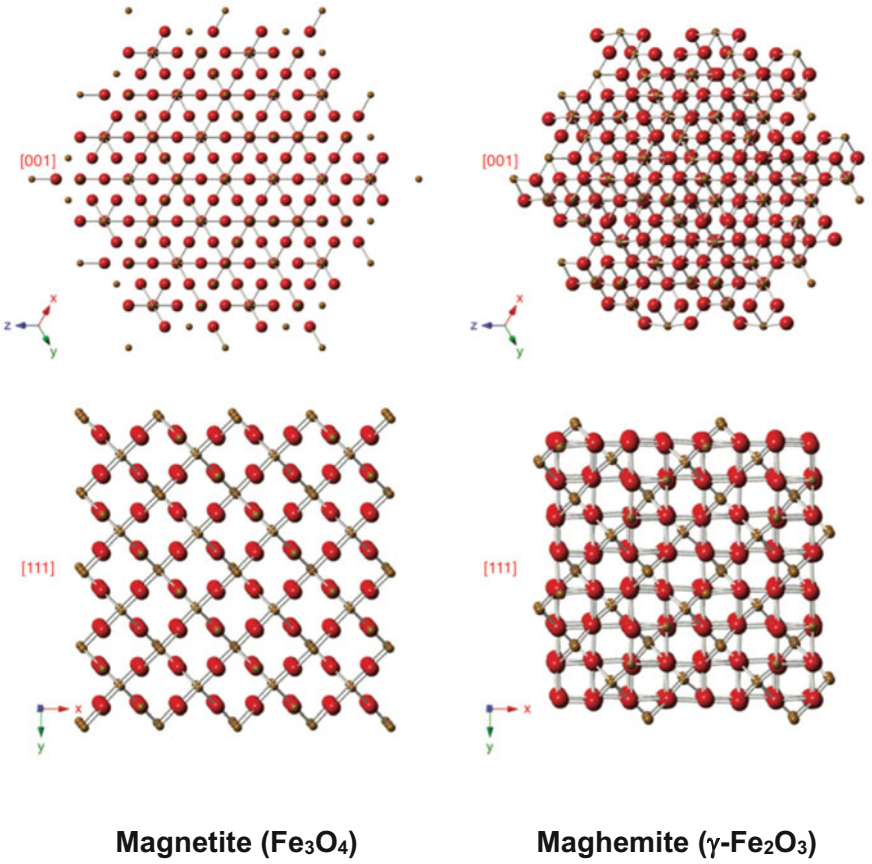

Fig. 47 Crystal structure of magnetite (Fe_3O_4) and maghemite (γ-Fe_2O_3) – reproduction from ref. [115]

amines, esters, halides, and alkenes. Terminal alkynes gave a mixture of alkanes and alkenes. Finally, after extraction, the catalyst layer could be reused without loss of reactivity for up to seven cycles.

In Situ Preparation of the Fe(0) NP Catalyst A 10 mL flask was charged with $FeCl_3$ (0.20 mmol, 33.1 mg) and THF (3.6 mL) in a glovebox. Under vigorous stirring, EtMgCl in THF (2 M, 0.80 mmol, 0.40 mL) was added dropwise. The resulting dark mixture was stirred at rt. for 30 min before use.

Hydrogenation of Alkynes with [Fe(0)]/IL-1/MeCN A 4 mL vial with screw cap and PTFE septum was charged with [BMIM][NTf_2] (IL-1) (150 μL) and 0.50 mL of the freshly prepared catalyst solution in a glove box and the mixture was stirred for 2 min before THF was evaporated under reduced pressure (oil pump). The vial was transferred back into the glove box, charged with an alkyne (0.50 mmol), dry acetonitrile (0.50 mmol), and dry n-heptane (0.50 mL), and

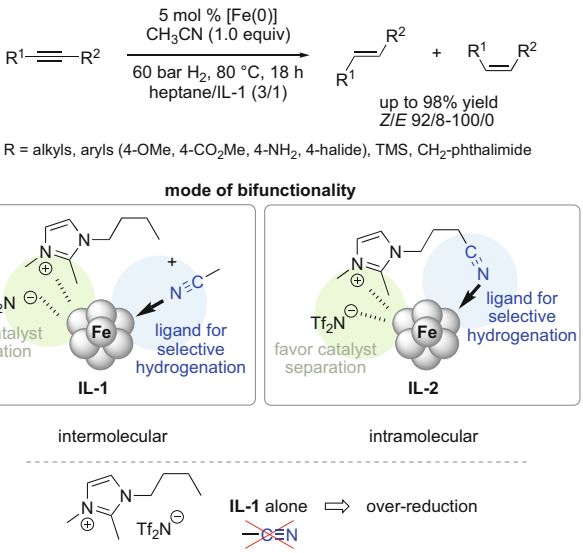

Fig. 48 Stereoselective Fe-catalyzed alkyne semi-hydrogenation in ionic liquids

then placed into a high-pressure reactor and punctured with a short needle, and the reactor was then sealed. The reactor was purged three times with hydrogen and pressurized with 53 bar of H_2, heated to 80°C by a heating jacket (resulting pressure 60 bar) and stirred with an external magnetic stirrer for 18 h. The reactor was then depressurized, the vial removed, the heptane phase separated by decantation, and the catalyst phase washed 2 × 1 mL with n-heptane. The product mixture was analyzed by GC and proton NMR. Quantifications were done via proton NMR vs. hexamethyldisiloxane as internal standard. For identification of *E/Z* stereochemistry of the resulting alkenes, the characteristic vinyl signals were analyzed and compared with literature data.

More recently, Corma and co-workers described a biomimetic approach using planar Fe(II)/(III) oxide nanoparticles supported on a slightly acidic material for the same reaction [117]. The support plays the role of a donor/acceptor entity, a functionality found in the active sites of hydrogenases. The nature of the support and the mode of preparation of the Fe-solid assembly are crucial, as only Fe deposed on TiO_2, ZrO_2, and ZnO by oxidative dispersion gave satisfactory results. Numerous alkynes have been reduced to the corresponding *Z*-alkenes, while aldehydes, with halides and nitro groups, remained unaffected. Although this method is not as selective as Lindlar-like catalysts, it is a useful tool for flow semi-hydrogenation of acetylene during ethylene manufacturing processes. The mechanism (Fig. 49) is believed to start with the adsorption of H_2 in the *n*FeOx catalytic sites, while adsorption of the alkyne occurs in both the Brønsted acid and *n*FeOx catalytic sites. Dihydrogen then dissociates heterolytically through

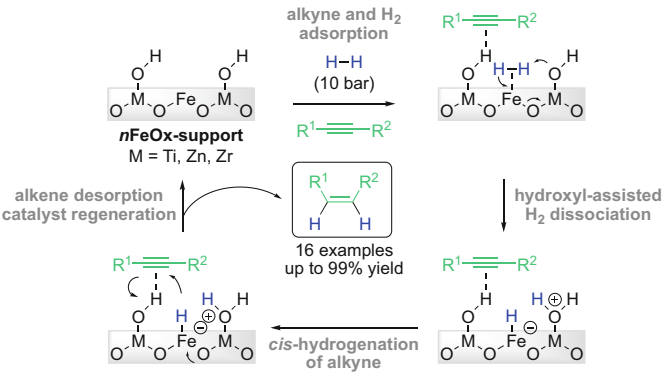

Fig. 49 Postulated mechanism for the *Z*-selective semi-hydrogenation of alkynes with nFeOx-supported catalysts

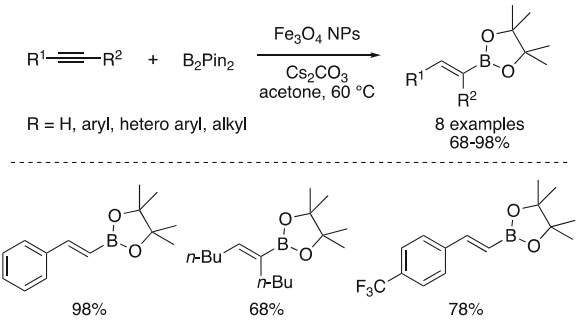

Fig. 50 Borylation of alkynes catalyzed by magnetic Fe NPs

a hydroxyl-assisted pathway. The alkyne is then *cis*-hydrogenated by the resulting hydride carried by the iron species, as well as the hydroxyl proton. Ti, Zn, or Zr are interesting metallic elements to constitute the solid support, as their electronegativity is substantially lower than Fe (1.3–1.6 vs. 1.8).

In 2014, Rawat et al. reported the regioselective borylation of alkynes to access *E*-vinylboronates (Fig. 50) [118]. Aryl, heteroaryl, as well as internal and external alkynes afforded good-to-excellent yields, while moderate yields were obtained with aliphatic substrates. The Fe_3O_4 NPs that perform this reaction could be isolated with an external magnetic field and reused without loss of reactivity (six recycles).

Magnetic silica-supported iron oxide (Fe_3O_4/SiO_2) NPs have also been employed for multicomponent syntheses of diazepines-2-carboxamides (Fig. 51) [119]. The reaction performed on model substrates showed significant improvement by using these NPs compared to non-supported Fe_3O_4 (92 vs. 35% yield, respectively). Yields ranged from 86 to 98% on 15 examples. After completion, the catalyst could be magnetically re-isolated, allowing its recycling for six cycles without loss of activity.

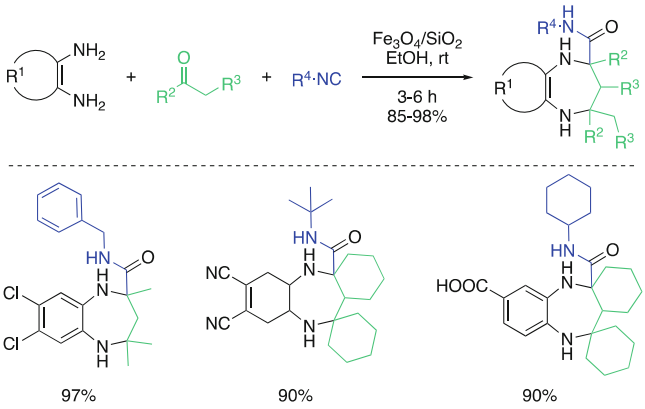

Fig. 51 Multicomponent diazepine-2-carboxamide synthesis catalyzed by Fe_3O_4/SiO_2 NPs

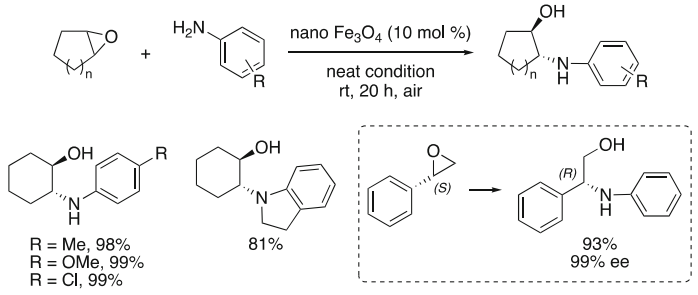

Fig. 52 Aminolysis of epoxides in presence of magnetic Fe_3O_4 NPs

A green route to access β-amino-alcohols, by ring-opening of epoxides with amines, has been reported by Kumar and co-workers [120]. Magnetically separable Fe_3O_4 NPs, under solvent-free and ambient conditions, catalyzed the reaction with high *trans*-selectivity. The NPs were recycled ten times with only a slight decrease in activity. In the case of chiral epoxides, a total inversion of the stereochemistry was noted, indicative of an S_N2-type mechanism (Fig. 52).

A synergistic effect between unmodified κ-carrageenan (a sulfated polysaccharide naturally present in red seaweed) and Fe_3O_4 nanoparticles has been observed on Michael additions of aldehydes, in their neat state, to nitroalkenes [121]. While the hybrid magnetic material showed good reactivity, individual species showed no catalytic activity. Despite a chiral environment induced by the polysaccharide, no enantioselectivity has been detected. Thus, the authors reported the functionalization of the hybrid material using a nonracemic proline derivative (**1**, Fig. 53), leading to good-to-excellent enantioselectivities.

Iron oxide-containing NPs have also been developed as recoverable, magnetically supported materials for asymmetric organocatalysis, such as those derived from L-proline, but are outside the scope of this chapter [122].

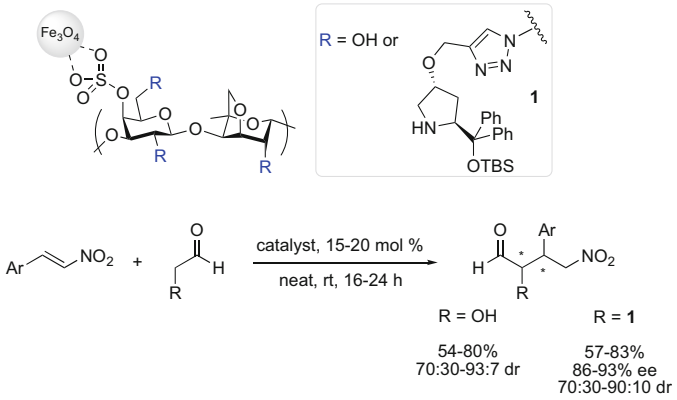

Fig. 53 Michael additions catalyzed by hybrid κ-carrageenan/Fe_3O_4 NPs

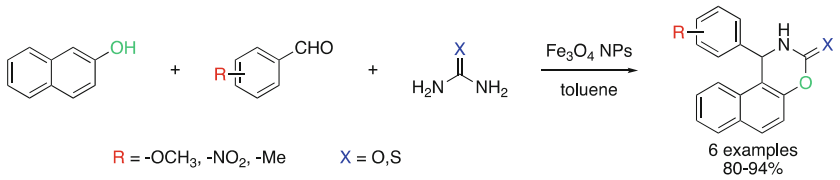

Fig. 54 Fe_3O_4 NPs applied to syntheses of benzoxazinones and benzthioxazinones

Common methods to prepare iron oxide-based NPs rely on toxic and, usually, reactive reductants such as $NaBH_4$ or hydrazine hydrate. Thus, more environmentally sound and safe routes are important to explore. Basavegowda et al. described a greener method for magnetite NP preparation using dried powder derived from naturally occurring *A. annua* leaves. A 5 mL aqueous filtrated infusion of the plant extract, rich in hydroxylated bioactive molecules, was mixed with 50 mL of a 2 mM aqueous solution of iron(III) chloride ($FeCl_3$), turning immediately into a black solution presumably forming Fe_3O_4 NPs [123], as the mechanism of NP formation by plant extracts remains unclear. A combination of several phytochemicals with redox properties (polyphenols, flavonoids, tannic acids, terpenoids, sugars, etc.) may be responsible for these reductions. Moreover, they can also act as capping agents that stabilize the particles [124]. These magnetite NPs have been tested in multicomponent syntheses of benzoxazinones and benzthioxazinones, compounds of interest given the variety of their biological activities. In one example, reaction of 2-naphthol with benzaldehyde derivatives and (thio)urea in the presence of 5 mol% of Fe_3O_4 NPs in refluxing toluene led to the desired products in good-to-excellent yields (Fig. 54).

11 Summary

This review highlights some of the advances in metal nanoparticle technology that have been made of late. Clearly, several of both the precious and base types of metals show considerable promise for inclusion into various NP formations, whether as their derived clusters or embedded on a solid support. Examples of mixed metal NPs are particularly exciting, as new synergistic activities have been uncovered leading to NP catalysts that show enhanced activities, suggestive of many more discoveries to come along these lines. Several reaction parameters addressed by the examples discussed herein, such as use of alternative reaction media (e.g., water, ILs, etc.), minimization of precious metals (e.g., platinoids), and attention to residual metals in products formed, all point to the potential for these catalysts to provide solutions to modern-day needs in catalysis. Indeed, based on these studies, the lines between homogeneous and heterogeneous catalysis have already begun to blur. And when considered together with environmental considerations taken into account in many of these reports, the future for NP technologies is not only very bright, but may figure prominently from the sustainability perspective of organic synthesis.

References

1. Liu L, Corma A (2018) Metal catalysts for heterogeneous catalysis: from single atoms to nanoclusters and nanoparticles. Chem Rev 118:4981–5079. https://doi.org/10.1021/acs.chemrev.7b00776
2. Phan NTS, van der Sluys M, Jones CW (2006) On the nature of the active species in palladium catalyzed Mizoroki–Heck and Suzuki–Miyaura couplings – homogeneous or heterogeneous catalysis, a critical review. Adv Synth Catal 348:609–679. https://doi.org/10.1002/adsc.200505473
3. Zhang D, Wang Q (2015) Palladium catalyzed asymmetric Suzuki–Miyaura coupling reactions to axially chiral biaryl compounds: chiral ligands and recent advances. Coord Chem Rev 286:1–16. https://doi.org/10.1016/j.ccr.2014.11.011
4. Lennox AJJ, Lloyd-Jones GC (2014) Selection of boron reagents for Suzuki–Miyaura coupling. Chem Soc Rev 43:412–443. https://doi.org/10.1039/C3CS60197H
5. Beletskaya IP, Cheprakov AV (2000) The heck reaction as a sharpening stone of palladium catalysis. Chem Rev 100:3009–3066. https://doi.org/10.1021/cr9903048
6. Rodríguez N, Goossen LJ (2011) Decarboxylative coupling reactions: a modern strategy for C–C-bond formation. Chem Soc Rev 40:5030–5048. https://doi.org/10.1039/C1CS15093F
7. Littke AF, Fu GC (2002) Palladium-catalyzed coupling reactions of aryl chlorides. Angew Chem Int Ed 41:4176–4211. https://doi.org/10.1002/1521-3773(20021115)41:22<4176::AID-ANIE4176>3.0.CO;2-U
8. Trzeciak AM, Augustyniak AW (2019) The role of palladium nanoparticles in catalytic C–C cross-coupling reactions. Coord Chem Rev 384:1–20. https://doi.org/10.1016/j.ccr.2019.01.008
9. Wu X-F, Neumann H, Beller M (2013) Synthesis of heterocycles via palladium-catalyzed carbonylations. Chem Rev 113:1–35. https://doi.org/10.1021/cr300100s
10. Gautam P, Bhanage BM (2015) Recent advances in the transition metal catalyzed carbonylation of alkynes, arenes and aryl halides using CO surrogates. Cat Sci Technol 5:4663–4702. https://doi.org/10.1039/C5CY00691K

11. Durand J, Teuma E, Gómez M (2008) An overview of palladium nanocatalysts: surface and molecular reactivity. Eur J Inorg Chem 2008:3577–3586. https://doi.org/10.1002/ejic.200800569
12. Torborg C, Beller M (2009) Recent applications of palladium-catalyzed coupling reactions in the pharmaceutical, agrochemical, and fine chemical industries. Adv Synth Catal 351:3027–3043. https://doi.org/10.1002/adsc.200900587
13. Narayanan R, El-Sayed MA (2003) Effect of catalysis on the stability of metallic nanoparticles: Suzuki reaction catalyzed by PVP-palladium nanoparticles. J Am Chem Soc 125:8340–8347. https://doi.org/10.1021/ja035044x
14. Handa S, Wang Y, Gallou F, Lipshutz BH (2015) Sustainable Fe–ppm Pd nanoparticle catalysis of Suzuki-Miyaura cross-couplings in water. Science 349:1087. https://doi.org/10.1126/science.aac6936
15. Lipshutz BH (2017) The 'Nano-to-Nano' effect applied to organic synthesis in water. Johns Matthey Technol Rev 61:196
16. Handa S, Jin B, Bora PP, Wang Y, Zhang X, Gallou F, Reilly J, Lipshutz BH (2019) Sonogashira couplings catalyzed by Fe nanoparticles containing ppm levels of reusable Pd, under mild aqueous Micellar conditions. ACS Catal 9:2423–2431. https://doi.org/10.1021/acscatal.9b00007
17. Feng J, Handa S, Gallou F, Lipshutz BH (2016) Safe and selective nitro group reductions catalyzed by sustainable and recyclable Fe/ppm Pd nanoparticles in water at room temperature. Angew Chem Int Ed 55:8979–8983. https://doi.org/10.1002/anie.201604026
18. Gabriel CM, Parmentier M, Riegert C, Lanz M, Handa S, Lipshutz BH, Gallou F (2017) Sustainable and scalable Fe/ppm Pd nanoparticle nitro group reductions in water at room temperature. Org Process Res Dev 21:247–252. https://doi.org/10.1021/acs.oprd.6b00410
19. Pang H, Gallou F, Sohn H, Camacho-Bunquin J, Delferro M, Lipshutz BH (2018) Synergistic effects in Fe nanoparticles doped with ppm levels of (Pd + Ni). A new catalyst for sustainable nitro group reductions. Green Chem 20:130–135. https://doi.org/10.1039/C7GC02991H
20. Sun J, Wang J, Feng X, Yamamoto Y, Almansour AI, Arumugam N, Kumar RS, Bao M (2018) Carboxylative Suzuki coupling reactions of benzyl chlorides with allyl pinacolborate catalyzed by palladium nanoparticles. Chin J Catal 39:1258–1262. https://doi.org/10.1016/S1872-2067(18)63045-1
21. Slack ED, Gabriel CM, Lipshutz BH (2014) A palladium nanoparticle–nanomicelle combination for the stereoselective semihydrogenation of alkynes in water at room temperature. Angew Chem Int Ed 53:14051–14054. https://doi.org/10.1002/anie.201407723
22. Jeanne-Julien L, Astier E, Lai-Kuen R, Genta-Jouve G, Roulland E (2018) Palladium nanoparticle-catalyzed stereoretentive cross-coupling of alkenyl sulfides with grignard reagents. Org Lett 20:1430–1434. https://doi.org/10.1021/acs.orglett.8b00208
23. Dictionary of Natural Products (2007) Chapman and Hall/CRC, Boca Raton. Internet resource
24. Heijnen D, Tosi F, Vila C, Stuart MCA, Elsinga PH, Szymanski W, Feringa BL (2017) Oxygen activated, palladium nanoparticle catalyzed, ultrafast cross-coupling of organolithium reagents. Angew Chem Int Ed 56:3354–3359. https://doi.org/10.1002/anie.201700417
25. Li X, Gong X, Li Z, Chang H, Gao W, Wei W (2017) Ligand- and copper-free Sonogashira and Heck couplings of (Het)aryl chlorides and bromides catalyzed by palladium nanoparticles supported on in situ generated Al(OH)3. RSC Adv 7:2475–2479. https://doi.org/10.1039/C6RA25416K
26. Gao W-Z, Xu Y, Chen Y, Fu W-F (2015) Highly efficient and selective photocatalytic reduction of nitroarenes using the Ni2P/CdS catalyst under visible-light irradiation. Chem Commun 51:13217–13220. https://doi.org/10.1039/C5CC04030B
27. Cai S, Duan H, Rong H, Wang D, Li L, He W, Li Y (2013) Highly active and selective catalysis of bimetallic Rh3Ni1 nanoparticles in the hydrogenation of nitroarenes. ACS Catal 3:608–612. https://doi.org/10.1021/cs300689w

28. Zhang J, Lu G, Cai C (2016) Chemoselective transfer hydrogenation of nitroarenes by highly dispersed Ni-Co BMNPs. Catal Commun 84:25–29. https://doi.org/10.1016/j.catcom.2016.05.023
29. Bódis J, Lefferts L, Müller TE, Pestman R, Lercher JA (2005) Activity and selectivity control in reductive amination of butyraldehyde over noble metal catalysts. Catal Lett 104:23–28. https://doi.org/10.1007/s10562-005-7431-4
30. Alonso F, Riente P, Yus M (2008) Hydrogen-transfer reductive amination of aldehydes catalysed by nickel nanoparticles. Synlett:1289–1292. https://doi.org/10.1055/s-2008-1072748
31. Jagadeesh R, Murugesan K, Beller M (2019) Reusable nickel nanoparticles-catalyzed reductive amination for selective synthesis of primary amines. Angew Chem Int Ed. https://doi.org/10.1002/anie.201812100
32. Sharma RK, Yadav M, Gaur R, Monga Y, Adholeya A (2015) Magnetically retrievable silica-based nickel nanocatalyst for Suzuki–Miyaura cross-coupling reaction. Cat Sci Technol 5:2728–2740. https://doi.org/10.1039/C4CY01736F
33. Handa S, Slack ED, Lipshutz BH (2015) Nanonickel-catalyzed Suzuki–Miyaura cross-couplings in water. Angew Chem Int Ed 54:11994–11998. https://doi.org/10.1002/anie.201505136
34. Sankar M, Dimitratos N, Miedziak PJ, Wells PP, Kiely CJ, Hutchings GJ (2012) Designing bimetallic catalysts for a green and sustainable future. Chem Soc Rev 41:8099–8139. https://doi.org/10.1039/C2CS35296F
35. Liu H, Mei Q, Li S, Yang Y, Wang Y, Liu H, Zheng L, An P, Zhang J, Han B (2018) Selective hydrogenation of unsaturated aldehydes over Pt nanoparticles promoted by the cooperation of steric and electronic effects. Chem Commun 54:908–911. https://doi.org/10.1039/C7CC08942B
36. Jang J, Byun S, Kim BM, Lee S (2018) Arylsilylation of aryl halides using the magnetically recyclable bimetallic Pd–Pt–Fe3O4 catalyst. Chem Commun 54:3492–3495. https://doi.org/10.1039/C7CC09926F
37. Heiss C, Schlosser M (2003) Organometallic control over the regiospecificity of functionalization reactions: 1,2,3-trifluorobenzene and bromo derivatives thereof as substrates. Eur J Org Chem 2003:447–451. https://doi.org/10.1002/ejoc.200390078
38. Luliński S, Serwatowski J (2003) Regiospecific metalation of oligobromobenzenes. J Org Chem 68:5384–5387. https://doi.org/10.1021/jo0340511
39. Zeng J (2012) A simple eco-friendly solution phase reduction method for the synthesis of polyhedra platinum nanoparticles with high catalytic activity for methanol electrooxidation. J Mater Chem 22:3170–3176. https://doi.org/10.1039/C1JM14413H
40. Pitre SP, Scaiano JC, Yoon TP (2017) Photocatalytic Indole Diels–Alder cycloadditions mediated by heterogeneous platinum-modified titanium dioxide. ACS Catal 7:6440–6444. https://doi.org/10.1021/acscatal.7b02223
41. Zamani A, Poursattar Marjani A, Nikoo A, Heidarpour M, Dehghan A (2018) Synthesis and characterization of copper nanoparticles on walnut shell for catalytic reduction and C-C coupling reaction. Inorg Nano-Met Chem 48:176–181. https://doi.org/10.1080/24701556.2018.1503676
42. He J, Zhang M, Primo A, García H, Li Z (2018) Selective photocatalytic benzene hydroxylation to phenol using surface-modified Cu_2O supported on graphene. J Mater Chem A 6:19782–19787. https://doi.org/10.1039/C8TA07095D
43. Rostovtsev VV, Green LG, Fokin VV, Sharpless KB (2002) A stepwise huisgen cycloaddition process: copper(I)-catalyzed regioselective "ligation" of azides and terminal alkynes. Angew Chem Int Ed 41:2596–2599. https://doi.org/10.1002/1521-3773(20020715)41:14<2596::AID-ANIE2596>3.0.CO;2-4
44. Tornøe CW, Christensen C, Meldal M (2002) Peptidotriazoles on solid phase: [1,2,3]-triazoles by regiospecific copper(I)-catalyzed 1,3-dipolar cycloadditions of terminal alkynes to azides. J Org Chem 67:3057–3064. https://doi.org/10.1021/jo011148j
45. Alonso F, Moglie Y, Radivoy G (2015) Copper nanoparticles in click chemistry. Acc Chem Res 48:2516–2528. https://doi.org/10.1021/acs.accounts.5b00293

46. Astruc D, Lu F, Aranzaes JR (2005) Nanoparticles as recyclable catalysts: the frontier between homogeneous and heterogeneous catalysis. Angew Chem Int Ed 44:7852–7872. https://doi.org/10.1002/anie.200500766
47. Alonso F, Moglie Y, Radivoy G, Yus M (2013) Alkenes as azido precursors for the one-pot synthesis of 1,2,3-triazoles catalyzed by copper nanoparticles on activated carbon. J Org Chem 78:5031–5037. https://doi.org/10.1021/jo400110m
48. Alonso F, Moglie Y, Radivoy G, Yus M (2011) Multicomponent click synthesis of 1,2,3-triazoles from epoxides in water catalyzed by copper nanoparticles on activated carbon. J Org Chem 76:8394–8405. https://doi.org/10.1021/jo2016339
49. Nador F, Volpe MA, Alonso F, Feldhoff A, Kirschning A, Radivoy G (2013) Copper nanoparticles supported on silica coated maghemite as versatile, magnetically recoverable and reusable catalyst for alkyne coupling and cycloaddition reactions. Appl Catal A Gen 455:39–45. https://doi.org/10.1016/j.apcata.2013.01.023
50. Alonso F, Moglie Y, Radivoy G, Yus M (2010) Multicomponent synthesis of 1,2,3-triazoles in water catalyzed by copper nanoparticles on activated carbon. Adv Synth Catal 352:3208–3214. https://doi.org/10.1002/adsc.201000637
51. Fu F, Martinez A, Wang C, Ciganda R, Yate L, Escobar A, Moya S, Fouquet E, Ruiz J, Astruc D (2017) Exposure to air boosts CuAAC reactions catalyzed by PEG-stabilized Cu nanoparticles. Chem Commun 53:5384–5387. https://doi.org/10.1039/C7CC02504A
52. Adenot A, Landstrom EB, Gallou F, Lipshutz BH (2017) Fe/ppm Cu nanoparticles as a recyclable catalyst for click reactions in water at room temperature. Green Chem 19:2506–2509. https://doi.org/10.1039/C7GC00883J
53. Pourjavadi A, Tajbakhsh M, Farhang M, Hosseini SH (2015) Copper-loaded polymeric magnetic nanocatalysts as retrievable and robust heterogeneous catalysts for click reactions. New J Chem 39:4591–4600. https://doi.org/10.1039/C4NJ02134G
54. Liu Y, Liu Z, Cui Y (2015) An efficient nanoparticle-supported and magnetically recoverable copper(I) catalyst for synthesis of furans from Ene-Yne-Ketone. Chin J Chem 33:175–180. https://doi.org/10.1002/cjoc.201400730
55. Wang K, Yang L, Zhao W, Cao L, Sun Z, Zhang F (2017) A facile synthesis of copper nanoparticles supported on an ordered mesoporous polymer as an efficient and stable catalyst for solvent-free Sonogashira coupling reactions. Green Chem 19:1949–1957. https://doi.org/10.1039/C7GC00219J
56. Sharma RK, Gaur R, Yadav M, Rathi AK, Pechousek J, Petr M, Zboril R, Gawande MB (2015) Maghemite-copper nanocomposites: applications for ligand-free cross-coupling (C−O, C−S, and C−N) reactions. ChemCatChem 7:3495–3502. https://doi.org/10.1002/cctc.201500546
57. Ugi I, Meyr R, Fetzer U (1959) Versammlungsberichte. Angew Chem 71:373–388. https://doi.org/10.1002/ange.19590711110
58. Ugi I, Steinbrückner C (1960) Über ein neues Kondensations-Prinzip. Angew Chem 72:267–268. https://doi.org/10.1002/ange.19600720709
59. Passerini M, Simone L (1921) Sopra gli isonitrili (I). Composto del p-isonitril-azobenzolo con acetone ed acido acetico. Gazz Chim Ital 51:126–129
60. Biginelli P (1891) Ueber aldehyduramide des acetessigäthers. Ber Dtsch Chem Ges 24:1317–1319. https://doi.org/10.1002/cber.189102401228
61. Biginelli P (1891) Ueber aldehyduramide des acetessigäthers. II. Ber Dtsch Chem Ges 24:2962–2967. https://doi.org/10.1002/cber.189102402126
62. Sharghi H, Shiri P, Aberi M (2014) A solvent-free and one-pot strategy for ecocompatible synthesis of substituted- benzofurans from various salicylaldehydes, secondary amines, and nonactivated alkynes catalyzed by copper(I) oxide nanoparticles. Synthesis 46:2489–2498. https://doi.org/10.1055/s-0034-1378206
63. Li J-H, Tang B-X, Tao L-M, Xie Y-X, Liang Y, Zhang M-B (2006) Reusable copper-catalyzed cross-coupling reactions of aryl halides with organotins in inexpensive ionic liquids. J Org Chem 71:7488–7490. https://doi.org/10.1021/jo061220j

64. Tang B-X, Wang F, Li J-H, Xie Y-X, Zhang M-B (2007) Reusable Cu2O/PPh3/TBAB system for the cross-couplings of aryl halides and heteroaryl halides with terminal alkynes. J Org Chem 72:6294–6297. https://doi.org/10.1021/jo070538o
65. Takale BS, Bao M, Yamamoto Y (2014) Gold nanoparticles (Au NPs) and gold nanopore (Au NPore) catalysts in organic synthesis. Org Biomol Chem 12:2005–2027
66. Haruta M, Yamada N, Kobayashi T, Iijima S (1989) Gold catalysts prepared by coprecipitation for low-temperature oxidation of hydrogen and of carbon monoxide. J Catal 115:301–309. https://doi.org/10.1016/0021-9517(89)90034-1
67. Fujita T, Guan P, McKenna K, Lang X, Hirata A, Zhang L, Tokunaga T, Arai S, Yamamoto Y, Tanaka N et al (2012) Atomic origins of the high catalytic activity of nanoporous gold. Nat Mater 11:775
68. Ferlin F, Cappelletti M, Vivani R, Pica M, Piermatti O, Vaccaro L (2019) Au@zirconium-phosphonate nanoparticles as an effective catalytic system for the chemoselective and switchable reduction of nitroarenes. Green Chem 21:614–626. https://doi.org/10.1039/C8GC03513J
69. Takale BS, Feng X, Lu Y, Bao M, Jin T, Minato T, Yamamoto Y (2016) Unsupported nanoporous gold catalyst for chemoselective hydrogenation reactions under low pressure: effect of residual silver on the reaction. J Am Chem Soc 138:10356–10364. https://doi.org/10.1021/jacs.6b06569
70. Takale BS, Tao SM, Yu XQ, Feng XJ, Jin T, Bao M, Yamamoto Y (2014) Exclusive chemoselective reduction of imines in the coexistence of aldehydes using AuNPore catalyst. Org Lett 16:2558–2561. https://doi.org/10.1021/ol500958p
71. Takale BS, Wang S, Zhang X, Feng X, Yu X, Jin T, Bao M, Yamamoto Y (2014) Chemoselective reduction of α,β-unsaturated aldehydes using an unsupported nanoporous gold catalyst. Chem Commun 50:14401–14404. https://doi.org/10.1039/C4CC07068B
72. Johnston P, Carthey N, Hutchings GJ (2015) Discovery, development, and commercialization of gold catalysts for acetylene hydrochlorination. J Am Chem Soc 137:14548–14557. https://doi.org/10.1021/jacs.5b07752
73. Han J, Liu Y, Guo R (2009) Facile synthesis of highly stable gold nanoparticles and their unexpected excellent catalytic activity for Suzuki−Miyaura cross-coupling reaction in water. J Am Chem Soc 131:2060–2061. https://doi.org/10.1021/ja808935n
74. Candu N, Dhakshinamoorthy A, Apostol N, Teodorescu C, Corma A, Garcia H, Parvulescu VI (2017) Oriented Au nanoplatelets on graphene promote Suzuki-Miyaura coupling with higher efficiency and different reactivity pattern than supported palladium. J Catal 352:59–66. https://doi.org/10.1016/j.jcat.2017.04.034
75. Thomas M, Sheikh MUD, Ahirwar D, Bano M, Khan F (2017) Gold nanoparticle and graphene oxide incorporated strontium crosslinked alginate/carboxymethyl cellulose composites for o-nitroaniline reduction and Suzuki-Miyaura cross-coupling reactions. J Colloid Interface Sci 505:115–129. https://doi.org/10.1016/j.jcis.2017.05.051
76. Nemygina NA, Nikoshvili LZ, Tiamina IY, Bykov AV, Smirnov IS, LaGrange T, Kaszkur Z, Matveeva VG, Sulman EM, Kiwi-Minsker L (2018) Au Core–Pd shell bimetallic nanoparticles immobilized within hyper-cross-linked polystyrene for mechanistic study of Suzuki cross-coupling: homogeneous or heterogeneous catalysis? Org Process Res Dev 22:1606–1613. https://doi.org/10.1021/acs.oprd.8b00272
77. Khodaei MM, Dehghan M (2019) A green and cost-effective approach for the production of gold nanoparticles using corn silk extract: a recoverable catalyst for Suzuki–Miyaura reaction and adsorbent for removing of dye pollutants. Polyhedron 162:219–231. https://doi.org/10.1016/j.poly.2019.01.060
78. Nasrollahzadeh M, Sajadi SM, Rostami-Vartooni A, Khalaj M (2014) Journey on greener pathways: use of Euphorbia condylocarpa M. bieb as reductant and stabilizer for green synthesis of Au/Pd bimetallic nanoparticles as reusable catalysts in the Suzuki and Heck coupling reactions in water. RSC Adv 4:43477–43484. https://doi.org/10.1039/C4RA07173E

79. Nasrollahzadeh M, Banaei A (2015) Hybrid Au/Pd nanoparticles as reusable catalysts for heck coupling reactions in water under aerobic conditions. Tetrahedron Lett 56:500–503. https://doi.org/10.1016/j.tetlet.2014.12.041
80. de Souza ROMA, Bittar MS, Mendes LVP, da Silva CMF, da Silva VT, Antunes OAC (2008) Copper-free Sonogashira reaction using gold nanoparticles supported on Ce2O3, Nb2O5 and SiO2 under microwave irradiation. Synlett 2008:1777–1780. https://doi.org/10.1055/s-2008-1078565
81. Nafria R, Luo Z, Ibáñez M, Martí-Sànchez S, Yu X, de la Mata M, Llorca J, Arbiol J, Kovalenko MV, Grabulosa A et al (2018) Growth of Au–Pd2Sn nanorods via galvanic replacement and their catalytic performance on hydrogenation and sonogashira coupling reactions. Langmuir 34:10634–10643. https://doi.org/10.1021/acs.langmuir.8b02023
82. Peshkov VA, Pereshivko OP, van der Eycken EV (2012) A walk around the A3-coupling. Chem Soc Rev 41:3790–3807. https://doi.org/10.1039/C2CS15356D
83. Ermolat'ev DS, Bariwal JB, Steenackers HPL, de Keersmaecker SCJ, Van der Eycken EV (2010) Concise and diversity-oriented route toward polysubstituted 2-aminoimidazole alkaloids and their analogues. Angew Chem Int Ed 49:9465–9468. https://doi.org/10.1002/anie.201004256
84. Xu Q, Rozners E (2005) Asymmetric synthesis of trans-3,4-dialkyl-γ-butyrolactones via an Acyl-Claisen and Iodolactonization route. Org Lett 7:2821–2824. https://doi.org/10.1021/ol050578j
85. Kidwai M, Bansal V, Kumar A, Mozumdar S (2007) The first Au-nanoparticles catalyzed green synthesis of propargylamines via a three-component coupling reaction of aldehyde, alkyne and amine. Green Chem 9:742–745. https://doi.org/10.1039/B702287E
86. Huang J-L, Gray DG, Li C-J (2013) A3-coupling catalyzed by robust Au nanoparticles covalently bonded to HS-functionalized cellulose nanocrystalline films. Beilstein J Org Chem 9:1388–1396. https://doi.org/10.3762/bjoc.9.155
87. Chen Y, Liu C, Abroshan H, Li Z, Wang J, Li G, Haruta M (2016) Phosphine/phenylacetylide-ligated Au clusters for multicomponent coupling reactions. J Catal 340:287–294. https://doi.org/10.1016/j.jcat.2016.05.023
88. Veisi H, Farokhi M, Hamelian M, Hemmati S (2018) Green synthesis of Au nanoparticles using an aqueous extract of stachys lavandulifolia and their catalytic performance for alkyne/aldehyde/amine A3 coupling reactions. RSC Adv 8:38186–38195. https://doi.org/10.1039/C8RA06819D
89. Carrettin S, Blanco MC, Corma A, Hashmi ASK (2006) Heterogeneous gold-catalysed synthesis of phenols. Adv Synth Catal 348:1283–1288. https://doi.org/10.1002/adsc.200606099
90. Gupta AK, Rhim CY, Oh CH, Mane RS, Han S-H (2006) Gold nanoparticle-catalysed [3 + 2] dipolar cycloaddition of 1,6-allenynebenzaldehydes: construction of polycyclic ring systems. Green Chem 8:25–28. https://doi.org/10.1039/B512034A
91. Gryparis C, Efe C, Raptis C, Lykakis IN, Stratakis M (2012) Cyclization of 1,6-enynes catalyzed by gold nanoparticles supported on TiO2: significant changes in selectivity and mechanism, as compared to homogeneous Au-catalysis. Org Lett 14:2956–2959. https://doi.org/10.1021/ol301212j
92. U. S. Department of Health and Human Services, Food and Drug Administration, Center for Drug Evaluation and Research (CDER), Center for Biologics Evaluation and Research (CBER) (2015) Q3D elemental impurities guidance for industry
93. Gniewek A, Trzeciak AM (2013) Rh(0) nanoparticles: synthesis, structure and catalytic application in Suzuki–Miyaura reaction and hydrogenation of benzene. Top Catal 56:1239–1245
94. Guha NR, Reddy CB, Aggarwal N, Sharma D, Shil AK, Bandna, Das P (2012) Solid-supported rhodium(0) nano−/microparticles: an efficient ligand-free heterogeneous catalyst for microwave-assisted Suzuki–Miyaura cross-coupling reaction. Adv Synth Catal 354:2911–2915

95. Kanuru VK, Humphrey SM, Kyffin JMW, Jefferson DA, Burton JW, Armbrüster M, Lambert RM (2009) Evidence for heterogeneous Sonogashira coupling of phenylacetylene and iodobenzene catalyzed by well defined rhodium nanoparticles. Dalton Trans 37:7602–7605
96. Karakulina A, Gopakumar A, Akçok I, Roulier BL, LaGrange T, Katsyuba SA, Das S, Dyson PJ (2016) A rhodium nanoparticle–Lewis acidic ionic liquid catalyst for the chemoselective reduction of heteroarenes. Angew Chem Int Ed 55:292–296
97. Yasukawa T, Miyamura H, Kobayashi S (2012) Polymer-incarcerated chiral Rh/Ag nanoparticles for asymmetric 1,4-addition reactions of arylboronic acids to enones: remarkable effects of bimetallic structure on activity and metal leaching. J Am Chem Soc 134:16963–16966
98. Yasukawa T, Suzuki A, Miyamura H, Nishino K, Kobayashi S (2015) Chiral metal nanoparticle systems as heterogeneous catalysts beyond homogeneous metal complex catalysts for asymmetric addition of arylboronic acids to α,β-unsaturated carbonyl compounds. J Am Chem Soc 137:6616–6623
99. Yasukawa T, Miyamura H, Kobayashi S (2014) Chiral metal nanoparticle-catalyzed asymmetric C–C bond formation reactions. Chem Soc Rev 43:1450–1461. https://doi.org/10.1039/C3CS60298B
100. Yasukawa T, Miyamura H, Kobayashi S (2016) Chiral ligand-modified metal nanoparticles as unique catalysts for asymmetric C–C bond-forming reactions: how are active species generated? ACS Catal 6:7979–7988. https://doi.org/10.1021/acscatal.6b02446
101. Yasukawa T, Kuremoto T, Miyamura H, Kobayashi S (2016) Asymmetric arylation of imines catalyzed by heterogeneous chiral rhodium nanoparticles. Org Lett 18:2716–2718
102. Miyamura H, Suzuki A, Yasukawa T, Kobayashi S (2018) Polysilane-immobilized Rh–Pt bimetallic nanoparticles as powerful arene hydrogenation catalysts: synthesis, reactions under batch and flow conditions and reaction mechanism. J Am Chem Soc 140:11325–11334. https://doi.org/10.1021/jacs.8b06015
103. Park JH, Kim E, Chung YK (2008) Heterobimetallic cobalt/rhodium nanoparticle-catalyzed carbonylative cycloaddition of 2-alkynylanilines to oxindoles. Org Lett 10:4719–4721
104. Park KH, Jung IG, Chung YK (2004) A Pauson−Khand-type reaction between alkynes and olefinic aldehydes catalyzed by rhodium/cobalt heterobimetallic nanoparticles: an olefinic aldehyde as an olefin and CO source. Org Lett 6:1183–1186
105. Park JH, Chung YK (2008) Cobalt–rhodium heterobimetallic nanoparticle-catalyzed reactions. Dalton Trans:2369–2378
106. Park JW, Chung YK (2015) Hydrogen-free cobalt–rhodium heterobimetallic nanoparticle-catalyzed reductive amination of aldehydes and ketones with amines and nitroarenes in the presence of carbon monoxide and water. ACS Catal 5:4846–4850
107. Choi I, Chun S, Chung YK (2017) Bimetallic cobalt–rhodium nanoparticle-catalyzed reductive amination of aldehydes with nitroarenes under atmospheric hydrogen. J Org Chem 82:12771–12777
108. Choi I, Chung H, Park JW, Chung YK (2016) Active and recyclable catalytic synthesis of indoles by reductive cyclization of 2-(2-nitroaryl)acetonitriles in the presence of Co–Rh Heterobimetallic nanoparticles with atmospheric hydrogen under mild conditions. Org Lett 18:5508–5511
109. Chandra D, Inoue Y, Sasase M, Kitano M, Bhaumik A, Kamata K, Hosono H, Hara M (2018) A high performance catalyst of shape-specific ruthenium nanoparticles for production of primary amines by reductive amination of carbonyl compounds. Chem Sci 9:5949–5956. https://doi.org/10.1039/C8SC01197D
110. Komanoya T, Kinemura T, Kita Y, Kamata K, Hara M (2017) Electronic effect of ruthenium nanoparticles on efficient reductive amination of carbonyl compounds. J Am Chem Soc 139:11493–11499. https://doi.org/10.1021/jacs.7b04481

111. Konnerth H, Prechtl MHG (2017) Selective hydrogenation of N-heterocyclic compounds using Ru nanocatalysts in ionic liquids. Green Chem 19:2762–2767. https://doi.org/10.1039/C7GC00513J
112. Chen F, Surkus A-E, He L, Pohl M-M, Radnik J, Topf C, Junge K, Beller M (2015) Selective catalytic hydrogenation of heteroarenes with N-graphene-modified cobalt nanoparticles (Co3O4–Co/NGr@α-Al2O3). J Am Chem Soc 137:11718–11724. https://doi.org/10.1021/jacs.5b06496
113. Chen F, Kreyenschulte C, Radnik J, Lund H, Surkus A-E, Junge K, Beller M (2017) Selective semihydrogenation of alkynes with N-graphitic-modified cobalt nanoparticles supported on silica. ACS Catal 7:1526–1532. https://doi.org/10.1021/acscatal.6b03140
114. Qi X, Liu X, Qu L-B, Liu Q, Lan Y (2018) Mechanistic insight into cobalt-catalyzed stereodivergent semihydrogenation of alkynes: the story of selectivity control. J Catal 362:25–34. https://doi.org/10.1016/j.jcat.2018.03.016
115. Wu W, Jiang CZ, Roy VAL (2016) Designed synthesis and surface engineering strategies of magnetic iron oxide nanoparticles for biomedical applications. Nanoscale 8:19421–19474. https://doi.org/10.1039/C6NR07542H
116. Gieshoff TN, Welther A, Kessler MT, Prechtl MHG, von Wangelin AJ (2014) Stereoselective iron-catalyzed alkyne hydrogenation in ionic liquids. Chem Commun 50:2261–2264
117. Tejeda-Serrano M, Cabrero-Antonino JR, Mainar-Ruiz V, López-Haro M, Hernández-Garrido JC, Calvino JJ, Leyva-Pérez A, Corma A (2017) Synthesis of supported planar iron oxide nanoparticles and their chemo- and stereoselectivity for hydrogenation of alkynes. ACS Catal 7:3721–3729. https://doi.org/10.1021/acscatal.7b00037
118. Rawat VS, Sreedhar B (2014) Iron-catalyzed borylation reactions of alkynes: an efficient synthesis of E-vinyl boronates. Synlett 25:1132–1136
119. Maleki A (2012) Fe3O4/SiO2 nanoparticles: an efficient and magnetically recoverable nanocatalyst for the one-pot multicomponent synthesis of diazepines. Tetrahedron 68:7827–7833. https://doi.org/10.1016/j.tet.2012.07.034
120. Kumar A, Parella R, Babu SA (2014) Magnetic nano Fe3O4 catalyzed solvent-free stereo- and regioselective -aminolysis of epoxides by amines; a green method for the synthesis of β-amino alcohols. Synlett 25:835–842
121. Mak CA, Ranjbar S, Riente P, Rodríguez-Escrich C, Pericas MA (2014) Hybrid magnetic materials (Fe3O4/k-Carrageenan) as catalysts for the michael addition of aldehydes to nitroalkenes. Tetrahedron 70:6169–6173
122. Firouzi-Haji R, Maleki A (2019) L-proline-functionalized Fe3O4 nanoparticles as an efficient nanomagnetic organocatalyst for highly stereoselective one-pot two-step tandem synthesis of substituted cyclopropanes. ChemistrySelect 4:853–857. https://doi.org/10.1002/slct.201802608
123. Basavegowda N, Magar KBS, Mishra K, Lee YR (2014) Green fabrication of ferromagnetic Fe3O4 nanoparticles and their novel catalytic applications for the synthesis of biologically interesting benzoxazinone and benzthioxazinone derivatives. New J Chem 38:5415–5420
124. Saif S, Tahir A, Chen Y (2016) Green synthesis of iron nanoparticles and their environmental applications and implications. Nano 6:209. https://doi.org/10.3390/nano6110209